The Gaussian streaming model and Convolution Lagrangian effective field theory

Zvonimir Vlah[a,b] **Emanuele Castorina**[c] **Martin White**[c,d]

[a]Stanford Institute for Theoretical Physics and Department of Physics, Stanford University, Stanford, CA 94306, USA

[b]Kavli Institute for Particle Astrophysics and Cosmology, SLAC and Stanford University, Menlo Park, CA 94025, USA

[c]Department of Physics, University of California, Berkeley, CA 94720

[d]Department of Astronomy, University of California, Berkeley, CA 94720

E-mail: zvlah@stanford.edu, ecastorina@berkeley.edu, mwhite@berkeley.edu

Abstract. We update the ingredients of the Gaussian streaming model (GSM) for the redshift-space clustering of biased tracers using the techniques of Lagrangian perturbation theory, effective field theory (EFT) and a generalized Lagrangian bias expansion. After relating the GSM to the cumulant expansion, we present new results for the real-space correlation function, mean pairwise velocity and pairwise velocity dispersion including counter terms from EFT and bias terms through third order in the linear density, its leading derivatives and its shear up to second order. We discuss the connection to the Gaussian peaks formalism. We compare the ingredients of the GSM to a suite of large N-body simulations, and show the performance of the theory on the low order multipoles of the redshift-space correlation function and power spectrum. We highlight the importance of a general biasing scheme, which we find to be as important as higher-order corrections due to non-linear evolution for the halos we consider on the scales of interest to us.

Contents

1   Introduction

The growth of the large-scale structure in the observed Universe arises due to gravitational collapse into dark-matter dominated potentials, tempered by the expansion of the Universe. A wealth of information can be encoded in the growth rate, including constraints on the expansion history, the nature of dark energy and modified gravity [1, 2]. There are several ways of studying the growth of structure, but perhaps the oldest and highest signal-to-noise measurement comes from observations of the anisotropy in the clustering of objects in redshift surveys. Since the redshift, from which one infers distance, contains a contribution from the line-of-sight velocity the clustering of objects in redshift surveys exhibits anisotropy [1, 3, 4], known as redshift-space distortions (RSD).

Over the last several decades measurements of the redshift-space clustering of galaxies have become increasingly precise (for example the measurements from the recently completed BOSS survey [5] have percent-level uncertainties on quasi-linear scales) allowing highly precise tests of the current paradigm but also posing a significant challenge for theorists seeking to model the data. As we prepare for the next generation of surveys we need models which are

able to model the redshift-space clustering of biased tracers at the percent level over a wide range of scales (to break degeneracies between parameters).

In this paper we shall attempt to model the low-order moments of the redshift-space clustering signal in configuration space, using models based upon Lagrangian perturbation theory (LPT; see below) and the effective field theory of large-scale structure (EFT [6–13]). LPT is one of the oldest and most successful analytic model for studying large-scale structure, and provides a simple connection to N-body simulations and peaks theory [14]. EFT is a consistent method for incorporating the effects of non-perturbative physics into perturbation theory by including a number of additional terms, with free parameters, whose structure is determined by the symmetries of the theory. Our focus here will be on increasing the precision with which we can predict the clustering moments on intermediate scales ($> 25\,h^{-1}\mathrm{Mpc}$), rather than on increasing the range of scales we predict. We believe this is a more appropriate use of techniques built upon perturbation theory. For an alternative route, see Ref. [15].

The outline of this paper is as follows. In the next section we review the context within which we will do our calculations: (Lagrangian) perturbation theory and the (Gaussian) streaming model. The next section describes the computation of each piece of the streaming model in terms of perturbation theory, including our bias model and the impact of small-scale physics which is not explicitly modeled. In section 4 we discuss the expected evolution of the correlation function, and the extent to which measurements in finite redshift slice can be interpreted as being at an "effective" redshift. We present some preliminary comparison of our results with N-body simulations in section 5, finding that we are limited by the accuracy of the simulations. Finally we conclude in section 6. A number of technical steps are relegated to a series of appendices. Appendix A reviews the derivation of the streaming model. Appendix B reviews the Fourier-space statistics. Appendix C details the computation of the time-derivative terms which enter in the velocity statistics. Appendix D presents a more general Lagrangian bias model which includes derivatives of the initial density field and shear terms. Appendix E compares our formalism to the distribution function formalism of Ref. [16].

2 Background

The next few subsections present some background to set the stage and our notation. First we review LPT and then the "streaming model". Some of the derivations or more technical details are relegated to appendices.

Our focus will be the prediction of the two-point function in redshift space, i.e. the correlation function:

$$\xi(\mathbf{s}) = \langle \delta(\mathbf{x})\delta(\mathbf{x} + \mathbf{s}) \rangle. \tag{2.1}$$

which depends on the separation, $s = |\mathbf{s}|$, and the cosine of the angle between the separation and the line-of-sight[1] $\mu \equiv \hat{\mathbf{s}} \cdot \hat{\mathbf{z}}$. Following common practice we project the μ dependence onto Legendre polynomials, $\mathcal{P}_\ell$,

$$\xi(s, \mu) = \sum_\ell \xi_\ell(s)\mathcal{P}_\ell(\mu) . \tag{2.2}$$

By symmetry, odd ℓ moments vanish. In linear theory, only $\ell = 0, 2, 4$ contribute; we will focus our model predictions on those moments.

---

[1]We adopt the "plane-parallel" approximation throughout, so that the line-of-sight (LOS) is chosen along a single Cartesian axis: $\hat{\mathbf{z}}$.

2.1 Lagrangian perturbation theory

The Lagrangian approach to cosmological structure formation was developed in [17–25] and traces the trajectory of an individual fluid element through space and time. For a fluid element located at position $\mathbf{q}$ at some initial time t_0, its position at subsequent times can be written in terms of the Lagrangian displacement field $\boldsymbol{\Psi}$,

$$\mathbf{x}(\mathbf{q}, t) = \mathbf{q} + \boldsymbol{\Psi}(\mathbf{q}, t), \tag{2.3}$$

where $\boldsymbol{\Psi}(\mathbf{q}, t_0) = 0$. Every element of the fluid is uniquely labeled by $\mathbf{q}$ and $\boldsymbol{\Psi}(\mathbf{q}, t)$ fully specifies the evolution. In what follows we shall suppress the time dependence of $\boldsymbol{\Psi}$ for notational convenience. Once $\boldsymbol{\Psi}(\mathbf{q})$ is known, the density field at any time is simply

$$1 + \delta(\mathbf{x}) = \int d^3q \, \delta_D[\mathbf{x} - \mathbf{q} - \boldsymbol{\Psi}(\mathbf{q})] \quad \Rightarrow \quad \delta(\mathbf{k}) = \int d^3q \, e^{i\mathbf{k}\cdot\mathbf{q}}\big(e^{i\mathbf{k}\cdot\boldsymbol{\Psi}(\mathbf{q})} - 1\big) \tag{2.4}$$

For tracers which are biased, the density is modulated by a function of the linear density field, the Laplacian of the linear density field and shear field at $\mathbf{q}$ (see §3). The evolution of $\boldsymbol{\Psi}$ is governed by $\partial_t^2 \boldsymbol{\Psi} + 2H\partial_t \boldsymbol{\Psi} = -\nabla\Phi(\mathbf{q} + \boldsymbol{\Psi})$. We shall work throughout in terms of conformal time, $d\eta = dt/a$, and write $\mathcal{H} = aH$ for the conformal Hubble parameter. The equation of motion is thus $\ddot{\boldsymbol{\Psi}} + \mathcal{H}\dot{\boldsymbol{\Psi}} = -\nabla\Phi(\mathbf{q} + \boldsymbol{\Psi})$, where overdots indicate derivatives w.r.t. conformal time. In LPT one finds a perturbative solution for $\boldsymbol{\Psi}$, $\boldsymbol{\Psi} = \boldsymbol{\Psi}^{(1)} + \boldsymbol{\Psi}^{(2)} + \boldsymbol{\Psi}^{(3)} + \cdots$, with the first order solution, linear in the density field, being the Zeldovich approximation [17]. Higher order solutions are specified in terms of integrals of higher powers of the linear density field [25, 26]. To these perturbative terms are then added a series of 'extra' terms, which encapsulate the effect of the small-scale physics which is missing in the perturbative treatment [12, 13].

2.2 The streaming model

The effects of super-cluster infall [3] on large scales, and virial motions within clusters on small scales, act to modify the clustering pattern observed in redshift space. Early models of this effect [4, 27–31], nowadays termed "dispersion models", were primarily phenomenological in nature and treated the two regimes independently. While successful at describing early survey data they do not describe the effects at the level of detail necessary for current and future surveys.

A closely related class of models, inspired by [32, 33], are streaming models which aim to jointly model the density and velocity field. The number of pairs of objects in real space is related to $1 + \xi$, so if one has a model for the probability, $\mathcal{P}$, that a pair with real-space, line-of-sight separation $r_\parallel$ will be observed with redshift-space, line-of-sight separation $s_\parallel$ then pair conservation implies

$$1 + \xi^s(s_\perp, s_\parallel) = \int dy \, [1 + \xi(\mathbf{r})] \, \mathcal{P}\left(y = s_\parallel - r_\parallel | \mathbf{r}\right) \tag{2.5}$$

Our focus will be on the Gaussian streaming model (GSM), as originally developed in [34–36] and discussed in [37–40]. In the GSM we assume that – for massive enough halos at sufficiently high redshifts – $\mathcal{P}$ can be well approximated by a Gaussian, so that the redshift-space correlation function can be written (see Appendix A)

$$1 + \xi^s(s_\perp, s_\parallel) = \int \frac{dy}{\sqrt{2\pi}\,\sigma_{12}} \, [1 + \xi] \exp\left\{-\frac{[s_\parallel - y - \mu v_{12}]^2}{2\sigma_{12}^2}\right\} \tag{2.6}$$

with $r = \sqrt{y^2 + s_\perp^2}$, $\mu = s_\parallel / \sqrt{s_\perp^2 + s_\parallel^2}$, ξ the real-space correlation function (of the biased tracer), v_{12} the mean, pairwise infall velocity and σ_{12} the pairwise dispersion. The correlation function, ξ, and the velocity moments (v_{12} and σ_{12}) are functions of r, though that dependence has been suppressed in Eq. (2.6).

An alternative asymptotic expansion to the GSM is the "Edgeworth streaming model" of Ref. [39]. This keeps higher orders in the cumulant expansion (e.g. Appendix A) which improves the performance of the model at smaller scales and for higher multipoles. Ref. [39] show that for the halo masses they probed innaccuracies in the perturbative expansion are more significant than the neglect of the higher-order cumulants in the GSM, suggesting that improving the ingredients in the GSM will yield the most benefit. This mirrors the conclusions of Ref. [34], and forms part of the motivation for this work.

Ref. [39] also explore a number of coarse-graining approaches for perturbative evaluation of the pieces of the GSM, an approach which has been furthered by Ref. [40]. As we will discuss later, smoothing the initial field can mimic some of the effects of EFT operators (e.g. it can reduce the rms displacement, which tends to be over-predicted by LPT) and hence improve the numerical agreement between perturbation theory and simulations. However there are couplings between the long- and short-scale modes which need to be "integrated out" which are not taken into account in the smoothing approach. The apparent need for different smoothing scales in different cumulants can be naturally explained by the structure of the EFT counter terms entering the calculation.

3 The model ingredients

In this section we review the predictions of "Lagrangian effective field theory" for the ingredients going into the streaming model described above. Much of this material has been well developed in the literature, so we shall present here only the main results. The reader is referred to Refs. [22–24, 36, 41] for the development of 'standard' LPT and Refs. [12, 13] for the effective field theory corrections. We shall closely follow the notation in Refs. [22, 36], in particular we define $\langle \delta(\mathbf{q}_1)\delta(\mathbf{q}_2) \rangle = \langle \delta_1 \delta_2 \rangle_c = \xi(\mathbf{q} = \mathbf{q}_1 - \mathbf{q}_2)$, $\Delta_i = \Psi_i(\mathbf{q}_1) - \Psi_i(\mathbf{q}_2)$ and

$$U_i^{mn} = \langle \delta_1^m \delta_2^n \Delta_i \rangle_c \quad , \quad A_{ij}^{mn} = \langle \delta_1^m \delta_2^n \Delta_i \Delta_j \rangle_c \quad , \quad W_{ijk} = \langle \Delta_i \Delta_j \Delta_k \rangle_c \tag{3.1}$$

with the shorthand notation $A_{ij} = A_{ij}^{00}$ and $U_i = U_i^{10}$.

All of the LPT results presented in the paper rely on an approximation where these kernels are time independent (as in an Einstein-de Sitter cosmology). This is a potential source of systematic error since in other cosmologies, including ΛCDM, the LPT kernels can be time dependent. The effect of this on the one-loop matter power spectrum is typically at a sub-percent level [42–44], but can reach 1% or more when also considering momentum statistics [44] i.e. pairwise velocities and velocity dispersions. These effects are thus of particular interest if sub-percent predictions of the statistics in redshift space are required, but will not dominate our error budget.

We shall present our description of biased tracers in Lagrangian space. We use a generalised approach where, in addition to the expansion in powers of the linear density field δ_L (Refs. [22, 23]), we include the shear of this field s_{ij} up to second order (see e.g. [45–55]) and an explicit derivative expansion starting with $(\nabla^2/\Lambda_L^2)\delta_L$ [47, 56–60]. The associated scale, $1/\Lambda_L$, is related to the typical size of the object we are describing (also called also

proto-halos). We shall refer to it as the Lagrangian radius of the halo. Thus we can write

$$1 + \delta_X(\mathbf{x}) = \int d^3q \; F\big[\delta(\mathbf{q}), \nabla^2\delta(\mathbf{q}), s^2(\mathbf{q})\big]\delta_D\big[\mathbf{x} - \mathbf{q} - \mathbf{\Psi}(\mathbf{q})\big] \tag{3.2}$$

with $s^2 = s_{ij}s_{ij}$. For more detailed description of the biasing model we refer the reader to Appendix D. After auto-correlating the field we keep the biasing terms up to quadratic order (in the bias expansion) and one loop in the perturbative description of the nonlinear dynamics. We denote the first two functional derivative of F w.r.t δ as b_1 and b_2, the functional derivative w.r.t. $\nabla^2\delta$ as b_{∇^2} and the functional derivative w.r.t. s^2 as b_{s^2}.

The corresponding terms of the general expansion in the Eulerian framework have been discussed in [47, 56–59] who also include third order terms. The precise relation of these Eulerian and Lagrangian biasing terms is not simple and parts of the third order Eulerian terms are dynamically produced from evolving the Lagrangian bias framework [45, 46, 50, 51, 61, 62]. We intend to return to this question in a future publication.

Alternatively, biasing of dark matter halos can be studied in a phenomenological framework like the excursion set model [49] or the theory of Gaussian peaks [14, 63, 64]. The derivative (or in general 'scale dependent bias') and tidal terms can be analytically derived within these frameworks leading to predictions for the corresponding bias coefficients. For example, the derivative terms arise in the peaks model as a consequence of the peak constraint imposed on the initial field when smoothed on the halo scale [53, 65, 66]. These predictions can be very useful in describing the time evolution and approximate values of these bias parameters, which can be used e.g. as priors in the EFT framework (see §3.5).

Finally, we note that the one-loop integrals that appear in the calculation of both the LPT and bias terms typically rely on the computation of 2D numerical integrals (with higher loops involving higher dimensional integration). It has been shown recently that all of these integrals can be recast in a convenient form where Hankel transforms can be used to speed up the computation (see e.g. Appendix B in Ref. [67] for the one-loop LPT expressions and Ref. [68] for discussion of bias and RSD terms). Some of our biasing terms are already expressed in this form (see Appendix D).

3.1 The real-space correlation function

The real-space correlation function for tracers which are locally biased in Lagrangian space is given as the integral

$$1 + \xi(r) = \int d^3q \; M_0(\mathbf{r}, \mathbf{q}) . \tag{3.3}$$

where [24, 36, 41]

$$
\begin{aligned}
M_0 = {}& \frac{1}{(2\pi)^{3/2}|A_{\mathrm{lin}}|^{1/2}} e^{-(1/2)(q_i - r_i)(A_{\mathrm{lin}}^{-1})_{ij}(q_j - r_j)} \\
& \times \bigg\{ 1 - \frac{1}{2}G_{ij}A_{ij}^{1-\mathrm{loop}} + b_1^2\xi_L + \frac{1}{2}b_2^2\xi_L^2 - 2b_1 U_i g_i + \frac{1}{6}W_{ijk}\Gamma_{ijk} - [b_2 + b_1^2]U_i^{(1)}U_j^{(1)}G_{ij} \\
& \quad - b_1^2 U_i^{11}g_i - b_2 U_i^{20}g_i - 2b_1 b_2\xi_L U_i^{(1)}g_i - b_1 A_{ij}^{10}G_{ij} \\
& \quad - b_{s^2}\left(G_{ij}\Upsilon_{ij} + 2g_i V_i^{10}\right) + b_{s^2}^2\zeta - 2b_1 b_{s^2}g_i V_i^{12} + b_2 b_{s^2}\chi^{12} \\
& \quad - \frac{1}{2}\alpha_\xi \mathrm{tr}G + 2b_{\nabla^2}\mathcal{B} + 2b_{\nabla^2}b_1\mathcal{B}_{2,i}g_i + \cdots \bigg\} .
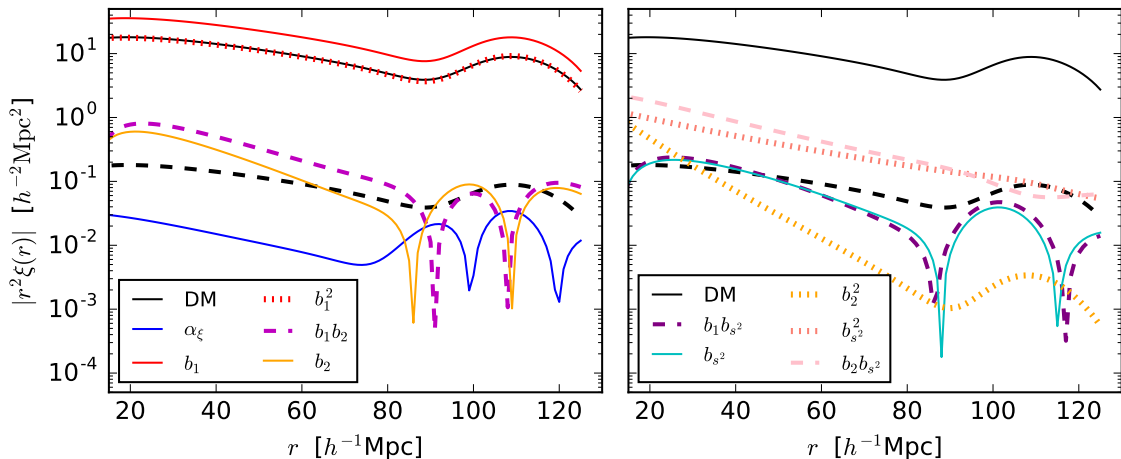\end{aligned}
\tag{3.4}
$$

Figure 1. The terms in Eq. (3.4) evaluated at $z = 0.8$ for illustration. The left panel shows the terms independent of b_{s^2} while the right panel shows the b_{s^2}-dependent terms. In each case the solid black line shows the DM-only correlation function (times r^2) corresponding to the "1" term in Eq. (3.4). To guide the eye on the relative size of the other terms, 1 per cent of this is shown as the dashed black line. It is clear that to first approximation $\xi(r) \approx (1 + b_1)^2 \xi_m(r)$ with corrections coming in at the few per cent level. It is also clear that the shear terms are at least as important as the b_2 terms.

and we have defined

$$
\begin{aligned}
g_i &= (A_{\rm lin}^{-1})_{ij}(q_j - r_j) \, , \quad G_{ij} = (A_{\rm lin}^{-1})_{ij} - g_i g_j \, , \\
\Gamma_{ijk} &= (A_{\rm lin}^{-1})_{ij} g_k + (A_{\rm lin}^{-1})_{ki} g_j + (A_{\rm lin}^{-1})_{jk} g_i - g_i g_j g_k \, .
\end{aligned}
\tag{3.5}
$$

Note our sign convention for g_i follows that of Ref. [36] and differs from that of Ref. [13] by a minus sign. This accounts for the difference in the sign of the Γ_{ijk} terms when comparing those two papers. It can be useful to have Fourier-space expressions as well, we relegate these to Appendix B.

The first 2 lines within the Eq. (3.4) are the predictions of standard Lagrangian perturbation theory. In the final line, the term depending on α is the "EFT term" which encapsulates the effects of unmodeled, small-scale physics. The numerical prefactor is conventional, and serves to standarzie the k-space expression. The b_{∇^2} terms on the last line come from the $\nabla^2 \delta$ bias, while the b_{s^2} terms on the third line are from the shear-dependence of the bias. Further details of the bias model, and expressions for $\mathcal{B}$, V, χ, ζ and Υ terms, are given in Appendix D.

The last three terms in Eq. (3.4) all have leading order contributions of the form $k^2 P_L(k)$. For this reason they are largely degenerate at the scales of interest and we can fit for just one (combined) free parameter, which we take to be the coefficient α_ξ. We emphasize that the degree of degeneracy is to some extent a numerical coincidence, since PT is an expansion in k/k_{NL} and bias is an expansion in k/Λ_L. The two scales are in principle separate, with k_{NL} typically larger than Λ_L. For this reason higher order terms in k/Λ_L could become important at k's for which the lowest order terms in k/k_{NL} are sufficient. The nature and degree of degeneracies at higher order remains an open question. Also note that our resummation scheme (keeping the $A_{\rm lin}$ in the exponent) breaks the degeneracies, but only by terms which

are higher order (see also the discussion in Ref. [13]; where a similar argument is made to drop some of the other EFT counter terms which would be degenerate with $k^2 P_L(k)$ to lowest order — similar approximations, neglecting higher angular dependencies, are made in [69]). We have verified that these differences are numerically small so henceforth we shall neglect the $\mathcal{B}$ terms.

Ref. [36] kept all of the 1-loop terms contributing to A_{ij} in the exponential, but here we have followed Ref. [13] and kept only the linear (Zeldovich) terms exponentiated while expanding the 1-loop terms into the $\{\cdots\}$. This is more consistent with our retention of only the lowest order EFT terms (while keeping the IR modes resummed). Note that our formalism allows for an alternative IR resummation procedure that was described in Appendix B of Ref. [13], which is similar to, albeit more general than, the procedure suggested in Ref. [69]. Similarly we have kept only terms up to second order in the linear theory power spectrum, $\mathcal{O}(P_L^2)$, in the $\{\cdots\}$ of Eq. (3.4). This implies that only the lowest order contributions to U_i are used in the terms indicated. We have found that this makes little difference numerically, but again is more self-consistent if we view the terms in Eq. (3.4) as an expansion in powers of P_L.

Fig. 1 shows the contributions to $r^2 \xi(r)$ evaluated at $z = 0.8$. The left panel shows the terms independent of b_{s^2} while the right panel shows the b_{s^2}-dependent terms. The dominant terms are the "1", b_1 and b_1^2 terms whose sum closely approximates $(1 + b_1)^2$ times the matter result. The dashed black line in each panel shows 1% of the matter result as a guide to the level of correction. We see that all of the terms (with the possible exception of b_2^2) are important at the 1% level. Naively the α_ξ term is smaller than our 1% mark, however we expect $\alpha_\xi \sim \mathcal{O}(10)$ given our normalization convention so that this term does become significant and can alter the width of the BAO peak (as well as modifying the small-scale correlation function).

3.2 The (mean) pairwise velocity

The mean, pairwise velocity is $v_{12} = v_{12,n}\hat{r}_n$ with

$$v_{12,n}(\mathbf{r}) = [1 + \xi(r)]^{-1} \int d^3q \; M_{1,n}(\mathbf{r}, \mathbf{q}) \; . \tag{3.6}$$

and [36]

$$
\begin{aligned}
M_{1,n} =& \frac{f}{(2\pi)^{3/2}|A_{\mathrm{lin}}|^{1/2}} e^{-(1/2)(q_i - r_i)(A_{\mathrm{lin}}^{-1})_{ij}(q_j - r_j)} \\
&\times \bigg\{ 2b_1\dot{U}_n - g_i\dot{A}_{in} + b_2\dot{U}_n^{20} + b_1^2\dot{U}_n^{11} - \frac{1}{2}G_{ij}\dot{W}_{ijn} - 2b_1 g_i\dot{A}_{in}^{10} \\
&+ 2b_1 b_2 \xi_L \dot{U}_n^{(1)} - [b_2 + b_1^2]\left(g_i U_i^{(1)}\dot{U}_n^{(1)} + g_i U_i^{(1)}\dot{U}_n^{(1)}\right) - b_1^2\xi_L g_i\dot{A}_{in}^{(1)} - 2b_1 G_{ij}U_i^{(1)}\dot{A}_{in}^{(1)} \\
&+ \alpha_v\nabla_n\xi_L - \alpha_v' g_n - 2b_{\nabla^2}\mathcal{B}_{2,n} \\
&+ b_{s^2}\left(2\dot{V}_n^{10} - g_i\dot{\Upsilon}_{in}\right) + b_1 b_{s^2}\dot{V}_n^{12} + \cdots \bigg\} \; ,
\end{aligned}
\tag{3.7}
$$

The dot notation and the relationship between the derivatives and base quantities is elucidated in Appendix C.

As above, the first 2 lines within the Eq. (3.7) are the predictions of Lagrangian perturbation theory, while the terms depending on α are the EFT terms which encapsulate the

small-scale physics and the extra terms are due to the scale-dependent and shear-dependent bias. As for ξ, we have truncated the expansion in Eq. (3.7) at second order in the linear theory power spectrum, P_L, which explains the use of $U_i^{(1)}$ and $A_{ij}^{(1)}$ in some terms.

3.3 The (pairwise) velocity dispersion

We decompose the velocity dispersion tensor into components parallel to and perpendicular to the separation. The cumulant[2] which enters Eq. (2.6) can be written as $\sigma_\parallel^2 = \hat{\sigma}_\parallel^2 - v_\parallel^2$ and $\sigma_\perp^2 = \hat{\sigma}_\perp^2$ where

$$\hat{\sigma}_\parallel^2 = \hat{\sigma}_{12,nm}^2 \hat{r}_n \hat{r}_m \ , \quad \hat{\sigma}_\perp^2 = \frac{1}{2}\hat{\sigma}_{12,nm}^2 \left(\delta_{nm}^K - \hat{r}_n \hat{r}_m \right) \ . \tag{3.8}$$

with

$$\hat{\sigma}_{12,nm}^2(\mathbf{r}) = [1 + \xi(r)]^{-1} \int d^3q \ M_{2,nm}(\mathbf{r},\mathbf{q}) \ . \tag{3.9}$$

and we have (see Ref. [36])

$$\begin{aligned}
M_{2,nm} =& \frac{f^2}{(2\pi)^{3/2}|A_{\rm lin}|^{1/2}} e^{-(1/2)(q_i-r_i)(A_{\rm lin}^{-1})_{ij}(q_j-r_j)} \\
& \times \left\{ [b_1^2 + b_2] \left(\dot{U}_n^{(1)}\dot{U}_m^{(1)} + \dot{U}_n^{(1)}\dot{U}_m^{(1)} \right) - 2b_1 \left(\dot{A}_{in}^{(1)}g_i\dot{U}_m^{(1)} + \dot{A}_{im}^{(1)}g_i\dot{U}_n^{(1)} \right) - \dot{A}_{im}^{(1)}\dot{A}_{jn}^{(1)}G_{ij} \right. \\
& \left. + \ddot{A}_{nm} + b_1^2\xi_L\ddot{A}_{nm}^{(1)} - 2b_1 U_i^{(1)}g_i\ddot{A}_{nm}^{(1)} + 2b_1\ddot{A}_{nm}^{10} + 2b_{s^2}\ddot{\Upsilon}_{mn} - \ddot{W}_{inm}g_i \right. \\
& \left. + \alpha_\sigma\delta_{nm} + \beta_\sigma\delta_{nm}\xi_L + \dots \right\} \ .
\end{aligned} \tag{3.10}$$

where above the first two lines in brackets $\{\cdots\}$ are the results from the usual Lagrangian perturbation theory, truncated to second order in P_L, and the terms in the last line are the EFT caunterterms. The first, constant, counterterm is a "contact" or "zero lag" term coming from all of the terms with a non-trivial $q \to \infty$ limit. In Fourier space these terms require an integration over all modes, including very high k modes. The second term, $\delta_{nm}\xi_L$, stands in for a number of terms which cancel the high-k sensitivity of the $\ddot{A}_{nm}$, $\ddot{A}_{nm}^{10}$ and $\ddot{W}_{inm}$ terms. In general there are counterterms with more complex structure, involving higher order Bessel functions, but they are largely degenerate on the scales where our 1-loop calculation is applicable (see also [13]) so we include only ξ_L above. We find these terms to be small, numerically. The predictions for σ_{ij}^2 are weakly dependent on the bias, except the dependence that comes through α_σ.

In Refs. [34, 36] it was noted that perturbation theory compares relatively well with numerical simulations on the shape of the pairwise velocity dispersion, but does much less well on the overall amplitude. The difference between the N-body measurements and the predictions of both Eulerian and Lagrangian perturbation theory is close to a constant. Here we see that the leading order EFT term, $\alpha_\sigma\delta_{ij}$, changes

$$\sigma_{ij}^2 \to \sigma_{ij}^2 + \alpha \ \frac{1 + \xi_{\rm mat}^{0-\rm loop}}{1 + \xi_{\rm halo}^{1-\rm loop}} \ \delta_{ij} \quad . \tag{3.11}$$

---

[2]The cumulant, σ^2, was used in the original GSM of Ref. [34] and in Ref. [39]. The non-cumulant version, $\hat{\sigma}^2$, was used in Ref. [36]. The differences manifest themselves primarily on small scales. We shall use the cumulant throughout (see Appendix A).

On large scales ($\xi \ll 1$) this is equivalent to adding a constant to both $\sigma_\parallel^2$ and $\sigma_\perp^2$ and drastically improves the agreement between theory and simulation[3]. This term corresponds to the lowest order correction for the finger of god effect suggested by Ref. [34]. Fingers of god are one of several small-scale effects missing from the perturbative treatment that can be handled using EFT methods. As noted above the α_σ counterterm has (zero lag) contributions from multiple terms: $\ddot{A}_{nm}$, $\ddot{A}_{nm}^{10}$ and $\ddot{\Upsilon}_{mn}$. Thus it can have a non-trivial bias dependence.

The α_σ term appears as a δ-function in Fourier space, as does the $\alpha_\sigma P_{\rm Zel}$ contribution (which corresponds to the leading P_{02} contributions in [70, 71], see also Appendix B). When considering M_0 and $M_{1,n}$, we have been assuming that the b_{∇^2} terms whose leading order contributions are $k^2 P_L$ are of similar size to the one-loop terms of similar form. In $M_{2,nm}$ these b_{∇^2} terms enter multiplied by terms like $U^{(1)}$ and hence can be dropped. This, in principle, breaks the degeneracy of the EFT counterterms and these derivative bias terms.

3.4 Impact of parameters

In this section we take a closer look at how the various parameters affect the predictions of the ingredients going into the GSM.

One of the earliest models of structure formation is the Zeldovich approximation, which does a good job of describing the growth of large scale structure into the non-linear regime (see e.g. Ref. [54]). Our theoretical model has several terms beyond the Zeldovich approximation, including 1-loop corrections in LPT, corrections for missing small-scale physics and a generalized, non-linear bias parameterization. In this subsection we will turn on these terms one at a time so that their impact on the clustering predictions can be assessed (see also Fig. 1).

Fig. 2 compares models for the real-space clustering in both Fourier (see Appendix B) and configuration space. To better show small deviations from the lowest order result we also show residuals compared to a reference model, and we take as the reference to be the Halo-Zeldovich model [72] in the form

$$P_{HZ}^{hh}(k) \equiv (1 + b_1)^2 P_{\rm Zel}^m(k) + {\rm const} \tag{3.12}$$

where $P_{\rm Zel}^m$ is the Zeldovich approximation for the mass power spectrum [21, 24, 72–75]. This model takes out the large-scale trends, allowing us to focus on the features in more detail. Notice that the const term in $P(k)$ transforms to a δ-function at zero lag in the correlation function, so our reference model for $\xi(r)$ is simply the Zeldovich matter correlation function times $(1 + b_1)^2$.

The blue line shows the effect of including lowest order Lagrangian bias (b_1) compared to simply multiplying the matter result by $(1 + b_1)^2$. We then add the EFT counter term (cyan line), which is degenerate with the b_{∇^2} terms, which affects the width of the peak in configuration space and adds additional power at higher k with undamped BAO oscillations in Fourier space. Both of these effects are expected from the nature of the term, $k^2 P_L(k)$ or a Laplacian of $\xi_L(r)$. We have chosen a very large value of α in order to emphasize the effect, and the sharpening of the peak is quite pronounced in the figure. Adding b_2 has little effect at the BAO peak but reduces the correlation function at smaller r. Including b_2 adds

---

[3]In principle this counter term can be negative and lead to $\sigma_{12}^2 < 0$ at small scales. We have not found this to be an issue in practice in our case. Should this become an issue one can keep just the linear part of σ_{12}^2, including the positive α_σ contribution, in the exponent and determinant and expand in the higher orders. This guarantees positive definiteness and introduces corrections only at higher orders higher than we are keeping.
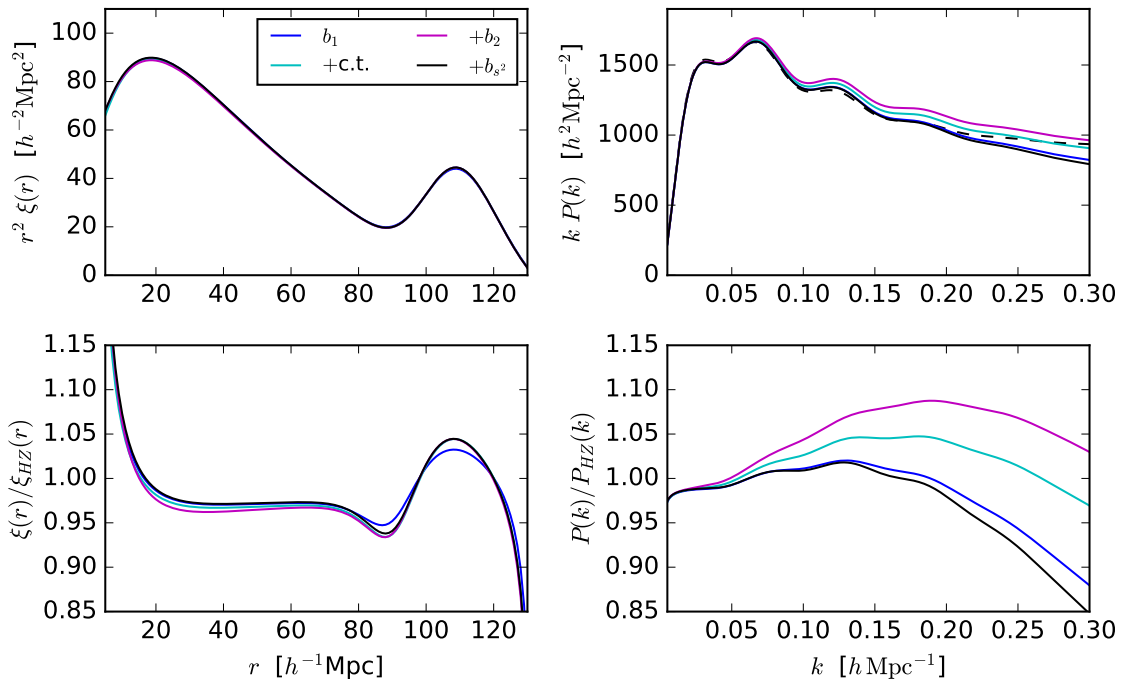
Figure 2. The contribution of different terms to the real-space 2-point function in (left) configuration and (right) Fourier space. The upper panels show $r^2 \xi(r)$ or $k P(k)$ while the lower panels show the ratio to a fiducial theory (taken to be the Halo-Zeldovich model, the black dashed line in the upper right panel; see text). The blue lines show the predictions with $b_1 = 1$ and all other parameters set to zero. Including the counter-term with $\alpha = -20$ (to emphasize the effect) generates the cyan line. Further adding $b_2 = 0.25$ gives the magenta line and finally adding $b_{s^2} = 0.5$ gives the black line.

significant power to $P(k)$ at high k. Finally we add b_{s^2}. The dominant effect in configuration space is a steepening of the correlation function, with a small change in the shape of the BAO peak. In Fourier space the shear terms modify high k significantly like the b_2 terms do.

We don't show the impact of the parameters on v_{12} and σ_{ij}^2 in a figure, as very few terms matter. On large scales v_{12} is proportional to $1 + b_1$, with the b_2 terms having very little effect. Either of the two counter terms causes a steepening of v_{12} at small r, which we will see improves agreement with the N-body and is important for matching the quadrupole to small scales (see discussion in Ref. [34]). The parallel and transverse components of the dispersion are very insensitive to any of the bias terms. The EFT counter term amounts to adding (or subtracting) a constant to both $\sigma_\parallel^2$ and $\sigma_\perp^2$, which helps improve agreement with the simulations and matches the finger-of-god correction implemented by Ref. [35].

3.5 The bias model and advantages of a Lagrangian formulation

We end this section with a few words about the bias model. When comparing to observations of biased tracers of the density field, choosing a suitably powerful and flexible bias model is clearly essential in order to not introduce biases into a fit. We have seen above that the relative size of even quite high-order bias terms is comparable to the affects of gravitational non-linearity at 1-loop or beyond.

The most general approach to bias is an EFT-inspired one (see [47, 56–59]). In fact, reasoning purely from symmetry is even more attractive for the bias model than for perturbative non-linearity because the ultimate theory we are wishing to describe in the case of bias is considerably more complex than the N-body problem. However, these approaches have the huge drawback of an explosion of undetermined parameters, especially as we push to higher order and include terms like $\nabla^2\delta$ and s_{ij} in our expansion. When the fitting range and accuracy are constrained, and only a small number of statistics are fit for, the difficulties of exploring multidimensional likelihood surfaces with strong degeneracies can become extreme.

While some gains can be made by including additional statistics (e.g. the 3-point functions) in the fits, we believe the appropriate approach is a combination of symmetry-based parameterizations with priors based on physical models of bias (e.g. Refs. [14, 76–79]). By allowing a flexible bias scheme, one can explore evidence from the data of violations of the simplest models. By including priors based on our decades of exploration of biasing in simulations and observations we can mitigate (to some extent) the difficulties inherent in any high-dimensional scheme.

In this approach a Lagrangian formulation of the problem appears to us to be highly beneficial. In cosmology the initial conditions are often considerably less complex than the late-time observations one is trying to describe. By formulating our bias model in terms of the Lagrangian field, and by disentangling the effects of evolution from complex bias, the Lagrangian formulation allows a more straightforward implementation of the programme described above.

4 Evolution and the effective-redshift approximation

Observations unavoidably measure clustering not at fixed time but along the past light-cone. Since the structure, and the bias of objects, evolves with time the measured correlation function is an "effective" one. If we define

$$X_{\text{eff}} = \frac{\int dz (dN/dz)^2 (H/\chi^2)\, X(z)}{\int dz (dN/dz)^2 (H/\chi^2)} \tag{4.1}$$

then on scales small compared to the scale of variation of dN/dz we measure $\xi_{\ell,\text{eff}}$ [80–82] which we interpret as $\xi_\ell(z_{\text{eff}})$, depending on parameters θ_{eff}. The accuracy of this approximation depends on the width of dN/dz and how rapidly the bias parameters (and the sample) are changing.

We use our analytic theory to investigate this issue, taking flat dN/dz of width $\Delta z = 0.1$ and 0.2. We have found that, for smoothly varying bias parameters, approximating $\xi_{\ell,\text{eff}}$ as $\xi_\ell(\theta_{\text{eff}}, z_{\text{eff}})$ induces very small errors, typically below one percent even for $\Delta z = 0.2$. This is true whether we take $\theta(z)$ to be constant, or impose an evolution based upon the peak-background split and fixed peak height [76, 79] or use the theory of excursion sets [76–79] or Gaussian peaks [14]. In making this comparison we need to assume a redshift-dependence of the counter terms, α_i. This is in principle arbitrary. While we know that the piece which absorbs the cut-off dependence must scale as $D^2(z)$, any finite pieces could evolve in a different way. Moreover, our α_i also account for ∇^2-bias terms, which are not expected to be proportional to $D^2(z)$. Despite these complications, we assume $\alpha_i \propto D^2(z)$, which is close to what is measured in N-body simulations [83].

For these assumptions, within our model, approximating $\xi_{\ell,\text{eff}}$ by $\xi_\ell(\theta_{\text{eff}}, z_{\text{eff}})$ induces sub-percent errors for both the monopole and the quadrupole. This suggests that, for such

smoothly evolving parameters, the neglect of light-cone effects is subdominant to higher order terms in the perturbative expansion or bias expansion. Of course, the redshift evolution of a real galaxy sample could be much more complicated than the models we have used, since several observational effects could start to play a role. Such situations would need to be investigated on a case-by-case basis, but the formalism above allows a rapid exploration of these approximations.

5   Comparison with simulations

We now make a preliminary comparison of the performance of the GSM, and its components predicted in perturbation theory, to the clustering of halos from N-body simulations. We find that we are currently limited by the size of systematic errors in the simulations, and so we defer a more detailed comparison to future work.

We make use of the halo catalogs[4] from the simulations described in Ref. [84]. Briefly, there were 4 realizations of a ΛCDM ($\Omega_m = 0.2648$, $\Omega_b h^2 = 0.02258$, $h = 0.71$, $n_s = 0.963$, $\sigma_8 = 0.8$) cosmology simulated with 4096^3 particles in a $4\,h^{-1}$Gpc box. The simulations were run with "derated" time steps chosen so that the matter power spectrum is accurate to better than 1% out to $k = 1\,h\,\mathrm{Mpc}^{-1}$ and halo masses were adjusted to match the halo abundance of a simulation with finer time steps.

We retrieved the halo catalogs for $z = 0.8$ and 0.55. The halos were defined by a friends-of-friends algorithm [85] with a linking length of 0.168 times the mean interparticle spacing (and the masses were redefined, as described in [84]).

Ref. [84] did not present convergence tests for the multipoles of the halo correlation function or power spectrum (though their Fig. 6 compares the monopole of the cross-correlation of the real- or redshift-space halo field with the real-space matter field). However the authors kindly made available two sets of simulations, one with derated time steps and one with time steps they consider "converged". By comparing the clustering of halos, with remapped masses, in the two simulations we can estimate[5] the effects of the derated time steps and hence a systematic error. The real-space power spectrum and the monopole of the redshift-space power spectrum show coherent, oscillatory residuals at the 1-2% level with slowly decreasing amplitude to $k \simeq 0.5\,h\mathrm{Mpc}^{-1}$. The power spectrum quadrupole shows oscillatory signals at just over 2%, with a feature near the acoustic scale. The effects are much larger in configuration space, with the ratio of the multipole moments differing from unity by 5% over much of the range of interest to us, with differences of more than 10% near $80\,h^{-1}$Mpc. The impact of these artifacts is likely highly dependent upon the use to which the simulations are being put, and quite difficult to assess without doing a detailed fit to a specific template. In our case, where we want to make precise predictions at large scales, they limit us to semi-qualitative comparisons below.

It is worthwhile to note that the total volume simulated, $256\,h^{-3}$Gpc^3, is equivalent to > 40 and > 25 full-sky surveys for redshift slices $0.5 < z < 0.6$ and $0.75 < z < 0.85$, respectively, and approximately $50\times$ the total volume of the BOSS survey [5]. The statistical errors from the simulations should thus be much smaller than those of any future survey

---

[4]The data are available at http://www.hep.anl.gov/cosmology/mock.html. Of the 5 realizations, the data for the first were corrupted so we used only the last 4.

[5]Our estimate is uncertain because the two simulations were evolved from different initial conditions, and thus some of the differences between the runs are due to sample variance and not methodological differences. However, the very large size of the boxes mitigates this uncertainty to some extent.

confined to a narrow redshift slice (see §4), and are dominated by systematic errors in the algorithms or physics missing from the simulations themselves.

We first computed the real- and redshift-space power spectrum and correlation function multipoles for halos in bins of mass ($12.5 < \lg M < 13.0$, $13.0 < \lg M < 13.5$ and $13.5 < \lg M < 14.0$; all masses in $h^{-1} M_\odot$) using the full periodic box, and used the average and scatter from the 4 boxes as our estimate of the signal and statistical uncertainty. We compute the power spectra in bins of width $0.0031 \, h \, \mathrm{Mpc}^{-1}$ and the correlation functions in bins of width $2 \, h^{-1} \mathrm{Mpc}$, which is small enough that effects due to binning are $\mathcal{O}(0.1\%)$ for the theories we wish to test. For the best measured, lowest mass, sample the statistical uncertainty on the redshift-space correlation function is at most a few percent on the scales of interest ($< 1\%$ for $s < 50 \, h^{-1} \mathrm{Mpc}$; $\sim 3\%$ at $s \simeq 80 \, h^{-1} \mathrm{Mpc}$; and $\sim 2 - 3\%$ for $s > 100 \, h^{-1} \mathrm{Mpc}$ for the redshift-space monopole for the lowest mass sample with smaller fractional errors for the quadrupole), with larger errors for the rarer halo samples (growing to tens of percent at high-s for the rarest samples). For the real-space correlation function the errors on the best-measured sample are $< 1\%$ for $r < 60 \, h^{-1} \mathrm{Mpc}$ and still $< 2\%$ across the acoustic peak. These rise to 4% across the acoustic peak for the highest mass sample. Similarly we computed the mean pairwise velocity and dispersion as a function of separation (in 100 bins equally spaced in r) for halos in the same mass bins. The mean pairwise velocity and dispersion were determined, statistically, to better than a percent on all relevant scales (though the systematic error from the derated time steps and halo mass is larger). The power spectrum used to generate the simulation intial conditions was not available to us, so we used CAMB[6] [86] to compute the linear theory power spectrum (using the cosmological parameters above) which is needed for the perturbation theory predictions.

We first checked that the lowest order streaming model is accurate when the "true" ingredients from the simulation are used. This updates the tests done in [34, 39]. Specifically we took the ξ, v_{12} and σ_{12} measured from the simulations and used the GSM as in Eq. (2.6) to generate the multipoles of the correlation function. As had been found previously, the GSM works well, lying within $\pm 2\%$ of the simulations on scales above $25 \, h^{-1} \mathrm{Mpc}$ for all masses and redshifts shown (i.e. within the systematic error budget of the simulations themselves). The monopole performs exceptionally well all the way down to $20 \, h^{-1} \mathrm{Mpc}$. Below this scale the model requires extrapolating $v_{12}(r)$ and $\sigma_i^2(r)$ to very small scales where it is hard to measure directly.

Now we check how well perturbation theory predicts each of the ingredients going into the streaming model. This updates the tests done in [34, 36, 39]. Overall the agreement between the theory and simulations is very good. We find this for all redshifts and mass bins that we have checked. Fig. 3 compares the model predictions for the real-space halo correlation function and power spectrum, the mean infall velocity and the velocity dispersions to the N-body results at $z = 0.55$ for halos with $12.5 < \lg M < 13.0$. We show this sample as it has the smallest statistical errors in the simulations, but the results for the other redshifts and mass sample are very similar. Errors on the N-body points are omitted for clarity. The statistical errors are approximately the size of the points. As we have argued above, the systematics errors are at the several per cent level.

Fig. 3 also compares the N-body and model results for the mean pairwise velocity, and again the agreement is very good. We also find that the model captures the scaling with mass and redshift well. Inclusion of the $\nabla \xi$ counter term improves the agreement with the N-body
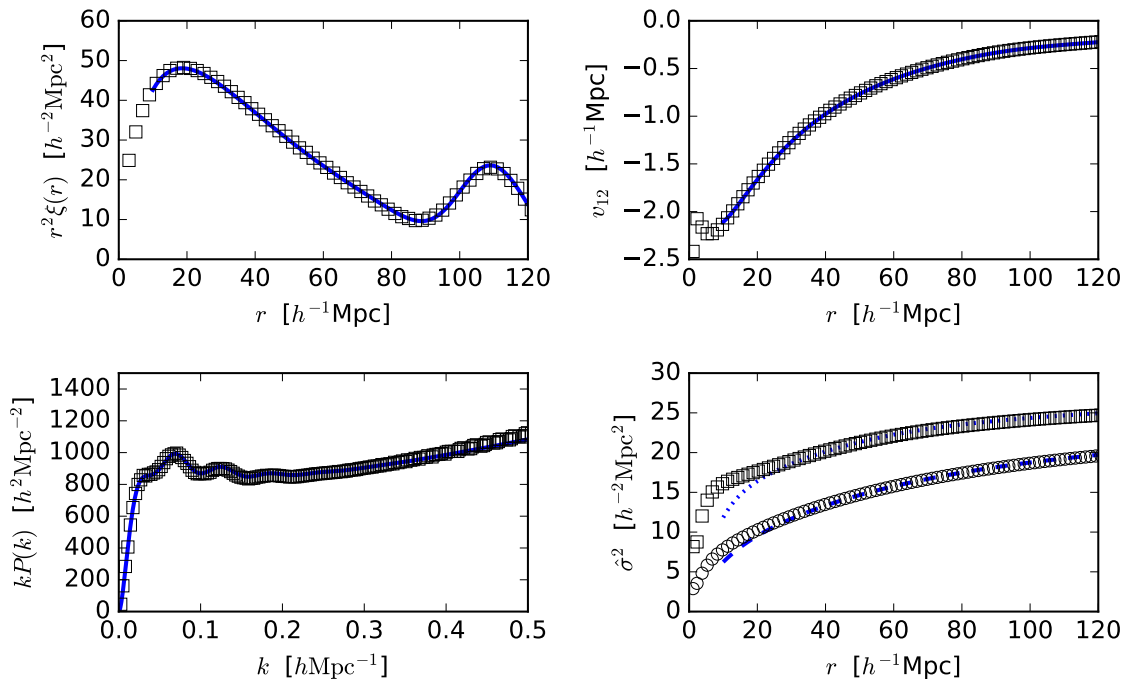

Figure 3. A comparison of the ingredients of the GSM, as computed in LEFT, with N-body simulations. We have chosen $z = 0.55$ and $12.5 < \lg M < 13.0$ as it has the smallest errors in the N-body (the other redshifts and mass ranges are qualitatively similar). (Top Left) The real-space correlation function, (Top Right) the mean infall velocity, (Bottom Left) the real-space power spectrum and (Bottom Right) the velocity dispersions parallel to (dotted) and transverse to (dashed) the separation vector. In each case the lines show the analytic prediction, while the points show the N-body results. The agreement on large scales is good, comparable to the numerical accuracy of the N-body results themselves.

Mass	b_1	b_2	b_{s^2}	α_ξ	α_v	α_σ
$12.5 < \lg M < 13.0$	0.68	-1.01	-0.92	-24	-52	-18
$13.0 < \lg M < 13.5$	1.28	-1.34	-0.14	-9	25	-3

Table 1. The best-fit parameters of the model shown in Fig. 4. These parameters have been fit 'by eye' and thus should be taken as indicative.

results on small scales, steepening the slope of v_{12} at small r. As has been noted before [34], correctly predicting the slope of v_{12} is crucial to modeling ξ_2 well in the GSM.

Finally Fig. 3 also compares the N-body and model predictions for the pairwise velocity dispersion ($\hat{\sigma}_i^2$) parallel and transverse to the separation vector. As noted in Ref. [34], the theory without the EFT terms mistestimates the dispersion. However the misestimate is very close to a constant, as expected from the lowest order EFT correction. This EFT correction is degenerate with the finger-of-god correction, as implemented by Ref. [35], which is also a non-linear effect. As such it does not increase the number of parameters in the model.

Finally we test the whole model. Fig. 4 shows the monopole and quadrupole of the
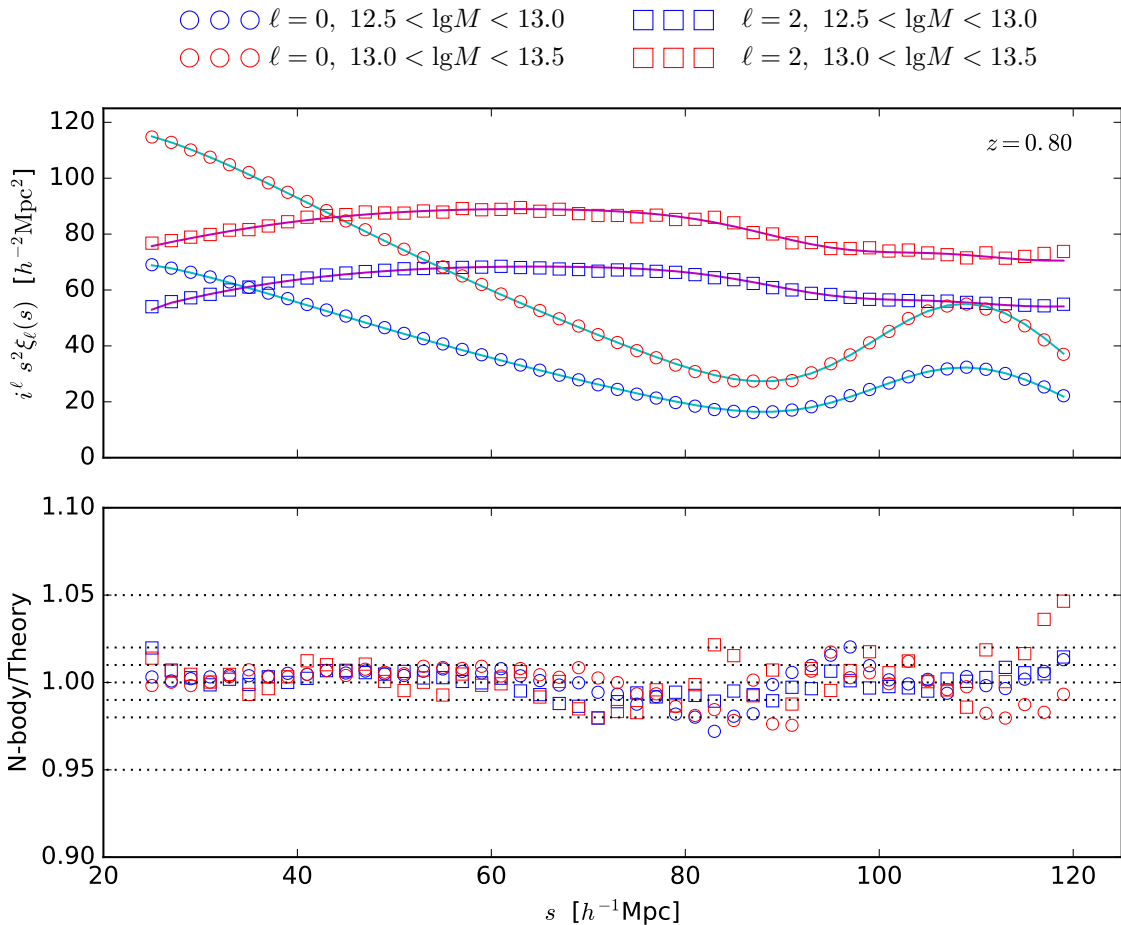
Figure 4. The comparison of the multipole moments of the redshift-space correlation function, $\xi_\ell(s)$, with the N-body results. The circles indicate the monople moment, the squares the quadrupole moment while blue points are for the $12.5 < \lg M < 13.0$ mass bin and red points the $13.0 < \lg M < 13.5$ bin. The fit is only to the points above $30\,h^{-1}\mathrm{Mpc}$, but the model clearly provides a good fit to the data below this scale as well.

redshift-space correlation function for two mass bins at $z = 0.8$ (the parameters are given in Table 1). This is the redshift bin for which we had the worst agreement with the ingredients, so gives the most pessimistic view of the model performance. We show the absolute agreement in the upper panel and the ratio of the N-body to the theory in the lower panel so that small deviations can be seen. Note in all cases the level of agreement is comfortably within the systematic errors of the simulations, which we estimate to be several per cent (we have shown ± 1, ± 2 and $\pm 5\%$ as dotted lines to guide the eye).

6 Conclusions

Redshift surveys by neccessity measure large-scale structure in redshift space, in which peculiar velocities sourced by large-scale gravitational potentials have induced anisotropic clustering. Measurement of these anisotropies allows us to probe the growth of large-scale structure,

breaking degeneracies in cosmological distance measures and providing a key test of general relativity and the gravitational instability paradigm on quasi-linear, cosmological scales.

In this paper we update earlier treatments of the Gaussian Streaming Model (GSM) and present tests against a new set of N-body simulations. We improve upon previous calculations of the ingredients in this model – the real-space correlation function, mean pairwise velocity and pairwise velocity dispersion – using a Lagrangian effective field theory with an extended bias model. We show that the Lagrangian approach provides a solid framework for studying large-scale structure, and provides a simple connection to N-body simulations and peaks theory. Effective field theory techniques provide a straightforward means of incorporating the effects of non-perturbative physics into perturbation theory by including additional terms whose structure is determined by the symmetries of the theory. The expressions for the ingredients, and the bias model, are new and present the most general expressions at the given order[7].

Throughout our focus has been on increasing the precision with which we can predict the clustering moments on intermediate scales ($> 25\,h^{-1}\mathrm{Mpc}$), rather than on increasing the range of scales we predict. We believe this is the most appropriate use of techniques built upon perturbation theory. Ultimately the precision of our model is limited by the neglect of 2-loop terms in the perturbative calculation, higher derivative orders in the EFT expansion, higher order terms in the bias expansion and the neglect of lightcone evolution. We find that these effects alter the predictions for the monopole and quadrupole moment of the correlation function and power spectrum at the per cent level on scales above $25 - 30\,h^{-1}\mathrm{Mpc}$.

The inclusion of 1-loop corrections to the Zeldovich approximation changes the clustering statistics by several per cent on large scales. The EFT terms encapsulate the effects of small-scale physics which is missing from the standard perturbative treatment. In $\xi(r)$ the primary effect is to change the width of the BAO peak and slightly decrease ξ at lower r. The EFT terms steepen v_{12} at small r, which is important in the streaming model in order to match the quadrupole. The EFT terms are most important for σ^2, where there is a large mismatch between the perturbative prediction and the N-body results [34, 36]. The difference is very close to a constant, independent of scale and orientation, which is also the behavior of the lowest-order EFT counter term. Such an offset was included in earlier versions of the GSM as a "finger-of-god" term, referring to a specific type of small-scale effect.

We find that a flexible bias model is at least as important as including the higher-order contributions to the evolution of clustering. The most general approach to bias is an EFT-inspired one, and reasoning purely from symmetry is highly attractive when describing the complex physics which leads to bias. We use a Lagrangian bias expansion up to the second order, including a derivative term and a shear term. This generates all the terms present in the corresponding third order Eulerian biasing expansion (see e.g. Refs. [47, 57–59]), although the latter has more freedom coming from an additional third order bias parameter in the real space two-point statistics. Adding the third order terms in Lagrangian space would yield the same number of free parameters in both Lagrangian and Eulerian picture. We argue that using a symmetry-based approach to bias, with priors set by theory and simulations, has many benefits. In such a scheme, a Lagrangian framework has multiple advantages over an Eulerian one (§3.5).

We have compared our theoretical calculations with 4 large N-body simulations [84], with a total simulated volume of $256\,h^{-3}\mathrm{Gpc}^3$. This volume, many times larger than accessible

---

[7]Code to evaluate these expressions is available at `https://github.com/martinjameswhite/CLEFT_GSM`.

observationally, leads to very small statistical errors. However the simulations were run with an approximate time-stepping scheme, which limits the overall accuracy to several percent on the statistics (and scales) of relevance here. With this caveat in mind, our model performs very well when compared to N-body simulations.

The model presented here achieves per cent level accuracy on the monopole and quadrupole of the correlation function and power spectrum on quasi-linear scales. This level of accuracy is likely sufficient for all upcoming surveys – going to higher order in perturbation theory or including additional EFT terms will yield little return. In order to push to smaller scales, detailed modeling of highly-nonlinear effects are required (e.g. Refs. [15, 87]) which will likely increase the number of parameters dramatically for even a small increase in dynamic range. Increasing the volume, to decrease the errors at fixed scale, requires increasing the redshift range and requires modeling of the evolution of the bias (in addition to survey non-idealities).

Our model works in a Lagrangian framework, with parameters that are easy to interpret within the context of the Gaussian peaks formalism or N-body simulations. Along with the LPT-based model for post-reconstruction BAO presented in [88], this formalism can be used to interpret the measurements from upcoming redshift surveys. The analytic nature of the calculation makes it possible rapidly explore changes in cosmology, and the flexible, parameterized bias model allows exploration of a wide range of effects with little effort. The analytic calculation can be used to set requirements for future grids of N-body models, both in terms of modeling the response surface for an emulator and in terms of which modes and which statistics need to be well converged.

Acknowledgments

A   The Gaussian Streaming Model

There are several routes to deriving the GSM, and its generalizations. The continuity equation allows us to relate the 2-point function in redshift space to a generating function [33, 34, 39]. If we recall that a shift in configuration space generates a phase in Fourier space, the generating function is

$$1 + \mathcal{M}(\mathbf{J}, \mathbf{r}) = \left\langle [1 + \delta(\mathbf{x})] \left[1 + \delta(\mathbf{x}')\right] e^{i\mathbf{J}\cdot\Delta\mathbf{u}} \right\rangle \tag{A.1}$$

where $\mathbf{r} = \mathbf{x} - \mathbf{x}'$, $\Delta\mathbf{u} = \mathbf{u}(\mathbf{x}') - \mathbf{u}(\mathbf{x})$, $\mathbf{u}$ is the velocity field in units of the Hubble expansion and $\mathbf{J} = k_\parallel \hat{z}$. Fourier transforming $1 + \mathcal{M}(k_\parallel \hat{z}, \mathbf{r})$ gives the redshift-space power spectrum. Using the cumulant expansion, i.e. expanding $\ln\left[1 + \mathcal{M}\right]$ in powers of $\mathbf{J}$, we have

$$1 + \mathcal{M} = \exp\left[\sum_{n=0}^{\infty} \frac{i^n}{n!} k_{i_1} \cdots k_{i_n} \mathcal{C}^{i_1\cdots i_n}\right] \tag{A.2}$$
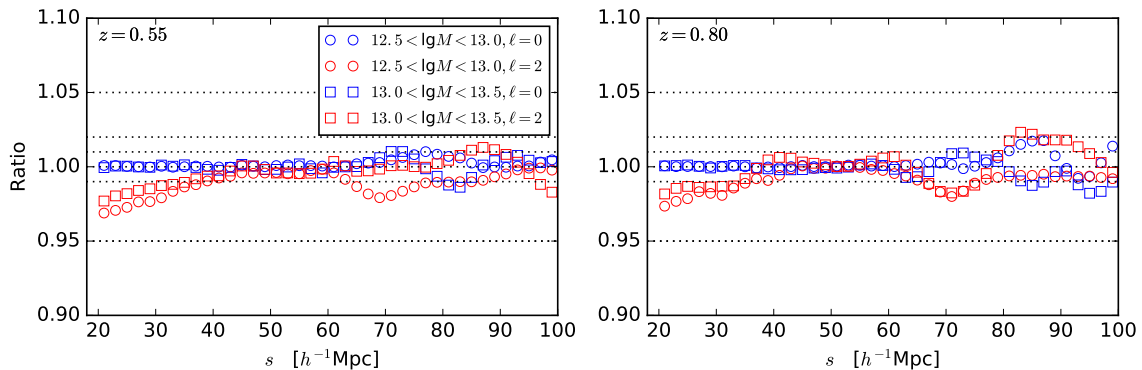
Figure 5. A test of the GSM using $\xi(r)$, $v_{12}(r)$ and $\sigma_{ij}^2(r)$ measured directly from the simulation. We have measured the ingredients of the GSM from the halo catalogs of the four N-body simulations, averaged them and then smoothed them to reduce noise. These were then used as ingredients in the GSM to compute $\xi_\ell(s)$. The figure shows the ratio of the $\xi_\ell(s)$ measured directly in the simulations (and smoothed to reduce noise) to the GSM prediction. The agreement on the monopole is excellent. The agreement on the quadrupole is within $\pm 2\%$ above $25\,h^{-1}\mathrm{Mpc}$.

where $C^{i_1\cdots i_n}$ are the density-weighted velocity cumulants. The first few cumulants are

$$C = \ln\left[1 + \xi\right] \tag{A.3}$$

$$C^i = \frac{\langle(1+\delta)(1+\delta')\Delta u^i\rangle}{1+\xi} \equiv v_{12}^i \tag{A.4}$$

$$C^{ij} = \frac{\langle(1+\delta)(1+\delta')\Delta u^i \Delta u^j\rangle}{1+\xi} - v_{12}^i v_{12}^j \equiv \sigma_{12}^{ij} \tag{A.5}$$

Keeping only terms through $n = 2$ in $1 + \mathcal{M}$, and performing the Fourier transform, the redshift-space correlation function is

$$1 + \xi(\mathbf{s}) = \int d^3 r \left[1 + \xi(\mathbf{r})\right] \int \frac{d^3 k}{(2\pi)^3} \; e^{-ik_i(s_i - r_i - v_{12}\hat{z}_i)} \; e^{-(1/2)k_i k_j \sigma_{12}\hat{z}_i\hat{z}_j} \tag{A.6}$$

The $d^3 k$ integral can be performed analytically and the result is the GSM, given in the main text. Higher order cumulants introduce higher corrections. These higher cumulants could be significant in case of large dispersion objects, and low redshifts. For example dark matter particles exhibit large FoG effects and some of these would be decomposed into these higher cumulants. Similar effects, but to smaller extent, might show up in smaller size halos, while we expect the higher terms to be less relevant for more massive halos and higher redshifts. The performance of the GSM when $\xi(r)$, $v_{12}(r)$ and $\sigma_{ij}^2(r)$ are measured from the simulations are shown in Fig. 5.

B Fourier space representation

The text focuses on the configuration-space description of the model and the clustering statistics, however on numerous occasions we have found it useful to examine the Fourier-space versions as well. In this appendix we give an example of the relevant formulae, referring the reader to Refs. [13, 24, 36, 41] for further details.

For example, the real-space, power spectrum (for $k \neq 0$) of halos can be written

$$P^{hh}(k) = \int d^3q \; e^{i\mathbf{k}\cdot\mathbf{q}} \exp\left[-\frac{1}{2}k_i k_j A_{ij}^{\rm lin}\right] \left\{1 - \frac{1}{2}k_i k_j A_{ij}^{1-\rm loop} - \frac{i}{6}k_i k_j k_l W_{ijk}^{1-\rm loop}\right.$$

$$- b_1\left(k_i k_j A_{ij}^{10} - 2ik_i U_i^{(1)}\right) + b_1^2\left(\xi_L + ik_i U_i^{11} - k_i k_j U_i^{(1)} U_j^{(1)}\right)$$

$$+ b_2\left(ik_i U_i^{20} - k_i k_j U_i^{(1)} U_j^{(1)}\right) + b_1 b_2\left(2ik_i U_i^{(1)}\xi_L\right) + b_2^2\left(\frac{1}{2}\xi_L^2\right)$$

$$- b_{s^2}\left(k_i k_j A_{ij}^{20} - 2ik_i V_i^{10}\right) + b_1 b_{s^2}\left(2ik_i V_i^{12}\right) + b_2 b_{s^2}\chi^{12} + b_{s^2}^2\zeta_L$$

$$\left. - \frac{1}{2}\alpha_\xi k^2 + i2b_{\nabla^2}\left(k_i \frac{\nabla^2}{\Lambda_L^2} U_i^{(1)}\right) + 2b_1 b_{\nabla^2}\left(\frac{\nabla^2}{\Lambda_L^2}\xi_L\right) + \dots\right\} + \text{``stochastic''}, \quad \text{(B.1)}$$

where "stochastic" represents the stochastic contributions to the power spectrum which we take to be a scale independent constant up to the order we work at. The ordering of the terms in this expression follows that for ξ in the main text, so that the correspondance is clear. The d^3q integral can be written in spherical polar coordinates, and the ϕ_q integral trivially gives 2π. The $\mathbf{k}\cdot\mathbf{q}$ in the exponent can be written as $kq\mu$, with the standard definitions of those terms. Expanding $k_i k_j A_{ij}$ gives terms going as μ^0 and μ^2. The integral over μ can then be written as a sum of spherical Bessel functions using the identities in Appendix A of Ref. [13] resulting finally in sums of 1D integrals:

$$P^{hh} = (1 - \tfrac{1}{2}\alpha_\xi k^2)P_{\rm zel} + P_{1-\rm loop} + b_1 P_{b_1} + b_1^2 P_{b_1^2} + b_2 P_{b_2} + b_1 b_2 P_{b_1 b_2} + b_2^2 P_{b_2^2} + b_{s^2} P_{b_{s^2}}$$

$$+ b_1 b_{s^2} P_{b_1 b_{s^2}} + b_2 b_{s^2} P_{b_2 b_{s^2}} + b_{s^2}^2 P_{(b_{s^2})^2} + 2b_{\nabla^2} P_{b_{\nabla^2}} + 2b_1 b_{\nabla^2} P_{b_1 b_{\nabla^2}} + \text{``const.''} + \dots \quad \text{(B.2)}$$

where $P_{\rm zel}$ and $P_{1-\rm loop}$ are the dark matter contributions, see e.g. Ref. [13]. For additional biasing terms we have terms of the form

$$P_x = 4\pi \int q^2 dq \; e^{-\frac{1}{2}k^2(X_L+Y_L)}\left(f_x^{(0)}(k,q)j_0(qk) + \sum_{n=1}^{\infty} f_x^{(n)}(k,q)\left(\frac{kY_L}{q}\right)^n j_n(qk)\right), \quad \text{(B.3)}$$

where integrands are:

term	$f_x^{(0)}$	$f_x^{(n)}$
b_1,	$-k^2\left(X^{10}+Y^{10}\right)$,	$-k^2\left(X^{10}+Y^{10}\right) + 2\left(nY^{10} - qU^{10}\right)/Y_L$,
b_1^2,	$\xi_L - k^2(U^{10})^2$,	$\xi_L - k^2(U^{10})^2 + \left(2n(U^{10})^2 - qU^{11}\right)/Y_L$,
b_2,	$-k^2(U^{10})^2$,	$-k^2(U^{10})^2 + \left(2n(U^{10})^2 - qU^{20}\right)/Y_L$,
$b_1 b_2$,	0,	$-2qU^{10}\xi_L/Y_L$,
b_2^2,	$\frac{1}{2}\xi_L^2$,	$\frac{1}{2}\xi_L^2$,
b_{s^2},	$-k^2\left(X^{20}+Y^{20}\right)$,	$-k^2\left(X^{20}+Y^{20}\right) + 2\left(nY^{20} - qV^{10}\right)/Y_L$,
$b_1 b_{s^2}$,	0,	$-qV^{12}/Y_L$,
$b_2 b_{s^2}$,	χ^{12},	χ^{12},
$(b_{s^2})^2$,	ζ_L,	ζ_L,
b_{∇^2},	0,	$-q\nabla^2 U^{10}/(\Lambda_L^2 Y_L)$,
$b_1 b_{\nabla^2}$,	$\nabla^2\xi_L/\Lambda_L^2$,	$\nabla^2\xi_L/\Lambda_L^2$,

The 1D integrals are Hankel transforms which can be done efficiently using FFTs [89] as was shown in [41]. The translation of the mean pairwise velocity and velocity dispersion terms is very similar.

C Time derivatives

We have followed Ref. [36] in writing the terms in Eqs. (3.7, 3.10) in terms of time derivatives. This is a shorthand, in which e.g. $\dot{A}_{ij}$ stands for $\langle \Delta_i \dot{\Delta}_j \rangle$. If we follow the normal convention and write each of the A_{ij} terms as $X\delta_{ij} + Y\hat{q}_i\hat{q}_j$, the time derivatives become:

$$f^{-1}\dot{X} = X^{(11)} + 2X^{(22)} + 4X^{(13)} \tag{C.1}$$

$$f^{-2}\ddot{X} = X^{(11)} + 4X^{(22)} + 6X^{(13)} \tag{C.2}$$

$$f^{-1}\dot{X}^{(10)} = (3/2)X^{(10)} \tag{C.3}$$

$$f^{-2}\ddot{X}^{(10)} = 2X^{(10)} \tag{C.4}$$

and analogously for the Y terms.

The displacement-density correlators behave as

$$f^{-1}\hat{q}_i\dot{U}_i = U^{(1)} + 3U^{(3)} \tag{C.5}$$

$$f^{-1}\hat{q}_i\dot{U}_i^{(20)} = 2U^{(20)} \tag{C.6}$$

$$f^{-1}\hat{q}_i\dot{U}_i^{(11)} = 2U^{(11)} \tag{C.7}$$

$$f^{-1}\hat{q}_i\dot{V}_i^{(10)} = 2V_i^{(10)} \tag{C.8}$$

$$f^{-1}\hat{q}_i\dot{V}_i^{(12)} = V_i^{(12)} \tag{C.9}$$

$$\tag{C.10}$$

while $f^{-1}\dot{\Upsilon}_{ij} = \Upsilon_{ij}$ and $f^{-2}\ddot{\Upsilon}_{ij} = \Upsilon_{ij}$.

Finally the W_{ijn} terms go as

$$f^{-2}\ddot{W}_{ijn} = 2W_{ijn}^{(112)} + 2W_{inj}^{(121)} + W_{nji}^{(211)}. \tag{C.11}$$

Note that only LPT contributions are considered in this section. In addition to the LPT terms we need to consider the counter terms which have a time dependent coefficient. This is taken into account in the main text above.

D Biasing expansion in the Lagrangian coordinates

When modeling the clustering of biased tracers to high precision, the modeling of the biasing can be of equal importance as the higher order corrections in perturbation theory (and the EFT terms) describing the nonlinear dynamics. Phrased in another way, the "cut-off" scale associated with the biasing can be larger than for dynamics, so we might need to keep higher order terms [57–60]. As we move into the future the tightest constraints will increasingly come from galaxies at higher redshifts (where surveys have the most volume) which will tend to be brighter and hosted by more massive halos for which we expect this will be even more true.

In our scheme we follow Ref. [22] in assuming local Lagrangian bias, but extend the model to include a dependence on derivative term $\nabla^2 \delta / \Lambda_L^2$ (with associated Lagrangian scale Λ_L) and the tidal shear tensor (see also [45–47, 50, 51, 54])

$$s_{ij}(\mathbf{k}) = \left(\frac{k_i k_j}{k^2} - \frac{1}{3}\delta_{ij} \right) \delta(\mathbf{k}) \tag{D.1}$$

as in Eq. (3.2). We assume that the biasing function is smooth, and can be Taylor expanded. We keep terms through second order in the field, neglecting the third order terms shear and local terms[8]. Explicitly, we can write for the overdensity of bias tracers in the Lagrangian coordinates

$$\delta_X(\mathbf{q}) = c_\delta \, \delta_L(\mathbf{q}) + c_{\delta^2} \left(\delta_L^2(\mathbf{q}) - \langle \delta^2 \rangle \right) + c_{s^2} \left(s^2(\mathbf{q}) - \langle s^2 \rangle \right)$$
$$+ c_{\nabla^2} \frac{\nabla_q^2}{\Lambda_L^2} \delta_L(\mathbf{q}) + \ldots + \text{``stochastic''}, \tag{D.2}$$

where "stochastic" stands for the stochastic contributions to the overdensity field of the biased tracers, and we have neglected the third biasing order terms like s^3, δs^3 etc. Fourier transforming F on $\nabla^2 \delta$, s^2, ... as well as δ we need to find the expectation value of exponentials such as [22–24]

$$\left\langle \exp\left[i \left(\mathbf{k} \cdot \mathbf{\Delta} + \lambda_1 \delta_1 + \lambda_2 \delta_2 + \eta_1 \nabla^2 \delta_1 + \eta_2 \nabla^2 \delta_2 + \zeta_1 s_1^2 + \zeta_2 s_2^2 + \cdots \right) \right] \right\rangle. \tag{D.3}$$

This can be evaluated using the cumulant expansion, and the terms depending on η_i, ζ_i, etc. can be Taylor expanded out of the exponential as is usually done for λ_i. As for the EFT counter terms, we treat the terms depending on $(\nabla^2/\Lambda_L^2)\delta$ and s^2 as "higher order", in this case in an expansion of k times the Lagrangian radius $(\sim 1/\Lambda_L)$ of the halo. When expanding these terms down from the exponential, keeping only linear contributions in the exponent, we truncate at $\mathcal{O}(P_L^2)$. We obtain the result given in the Eq. (3.4). The usual bias terms (due to the local Lagrangian bias) can be expressed in terms of linear correlation function $\xi_L = \langle \delta_1 \delta_2 \rangle_c$ and correlatiors

$$U_i^{10} = \langle \delta_1 \Delta_i \rangle_c, \quad U_i^{20} = \langle \delta^2 \Delta_i \rangle_c, \quad U_i^{11} = \langle \delta_1 \delta_2 \Delta_i \rangle_c, \quad A_{ij}^{10} = \langle \delta \Delta_i \Delta_j \rangle_c \quad . \tag{D.4}$$

for which expressions are given in Refs. [22–24]. To lowest order the $\nabla^2 \delta$ terms introduce only two new correlators:

$$\left\langle \nabla^2 \delta(\mathbf{q}_1) \delta(\mathbf{q}_2) \right\rangle \qquad \text{and} \qquad \left\langle \nabla^2 \delta(\mathbf{q}_1) \Psi_i^{(1)}(\mathbf{q}_2) \right\rangle. \tag{D.5}$$

Calling these $\mathcal{B}_i$ we have

$$\mathcal{B}_1(q) \equiv -\nabla^2 \xi_L(q) = \int \frac{k^2 \, dk}{2\pi^2} \, k^2 P_L(k) W(k; R) \, j_0(kq), \tag{D.6}$$

$$\mathcal{B}_{2,i}(q) \equiv -\nabla_i \xi_L(q) = \hat{q}_i \int \frac{k^3 \, dk}{2\pi^2} \, P_L(k) \, j_1(kq) \tag{D.7}$$

where W is a smoothing window which we shall not need explicitly. Note the similarity of $\mathcal{B}_1$ to the EFT counter term, which is $k^2 P_L(k)$ in Fourier space [13]. For this reason we shall not include this term in our model, as discussed in more detail in §3.1.

---

[8]We note that, by construction, the field ψ introduced in Ref. [47] vanishes in the initial conditions. This term arises (deterministically) due to evolution, so it does not have a biasing coefficient.

We note that including third order shear terms s^3 and δs^3, interestingly, leads to the trivial contributions in the sense that no new biasing parameters are needed. Specifically, we find that terms like $V_i^{11} = \langle s_1^2 \delta_{L1} \Delta_i \rangle_c$, which involve s^2 and δ at the same point and which would have given rise to new bias coefficients, vanish. Thus up to $\mathcal{O}(\delta^4)$ we have

$$V_i^{10} = \langle s^2 \Delta_i \rangle_c, \quad V_i^{12} = \langle s_1^2 \delta_2 \Delta_i \rangle_c, \quad \Upsilon_{ij} = \langle s^2 \Delta_i \Delta_j \rangle_c \tag{D.8}$$

and

$$\zeta = \langle s_1^2 s_2^2 \rangle_c, \quad \chi^{12} = \langle s_1^2 \delta_2^2 \rangle_c, \tag{D.9}$$

where we have

$$\chi^{12} = \frac{4}{3} \left[\int \frac{k^2 \, dk}{2\pi^2} P(k) \, j_2(kq) \right]^2, \tag{D.10}$$

and similarly the expression[9] for ζ can be found in [54]. The shear correlators introduce new combinations. Some of these terms can be written as products of integrals of P_L, viz

$$V_i^{12} = 2\hat{q}_i \int \frac{k \, dk}{2\pi^2} \, P_L(k) \left[\frac{4}{15} j_1(kq) - \frac{2}{5} j_3(kq) \right] \int \frac{k^2 \, dk}{2\pi^2} P_L(k) \, j_2(kq), \tag{D.11}$$

and similarly

$$\Upsilon_{mn} = 2 \left\langle s_{1,ij}^2 \Psi_{2,m} \right\rangle \left\langle s_{1,ij}^2 \Psi_{2,n} \right\rangle = 2 \left\{ \delta_{mn} \left(2\mathcal{J}_3^2 \right) + \hat{q}_m \hat{q}_n \left(3\mathcal{J}_2^2 + 4\mathcal{J}_2 \mathcal{J}_3 + \right. \right.$$
$$\left. \left. 2\mathcal{J}_2 \mathcal{J}_4 + 2\mathcal{J}_3^2 + 4\mathcal{J}_3 \mathcal{J}_4 + \mathcal{J}_4^2 \right) \right\} \tag{D.12}$$

where we have defined [54]

$$\mathcal{J}_2 = \int \frac{k \, dk}{2\pi^2} P_L(k) \left[\frac{2}{15} j_1(kq) - \frac{1}{5} j_3(kq) \right] \tag{D.13}$$

$$\mathcal{J}_3 = \int \frac{k \, dk}{2\pi^2} P_L(k) \left[-\frac{1}{5} j_1(kq) - \frac{1}{5} j_3(kq) \right] \tag{D.14}$$

$$\mathcal{J}_4 = \int \frac{k \, dk}{2\pi^2} P_L(k) \, j_3(kq) \tag{D.15}$$

Finally, $V_i^{10} = \langle s^2 \Delta_i \rangle_c$ which we can write

$$V_i^{10} = \left\langle s^2(\mathbf{q}_1) \Psi_i^{(2)}(\mathbf{q}_2) \right\rangle_c = -\frac{2\hat{q}_i}{7} \int \frac{k \, dk}{2\pi^2} Q_{s^2}(k) \, j_1(kq) \tag{D.16}$$

with

$$Q_{s^2}(k) = \frac{k^3}{4\pi^2} \int dr \, P_L(kr) \int dx \, P_L(k\sqrt{y}) Q_{s^2}(r, x), \tag{D.17}$$

where we have followed Ref. [22] and written $y = 1 + r^2 - 2rx$ and have defined

$$Q_{s^2}(r, x) = \frac{r^2(x^2 - 1)(1 - 2r^2 + 4rx - 3x^2)}{y^2}. \tag{D.18}$$

---

[9]There is a typo in Eq. (A6) of Ref. [54]: the coefficient of the $\mathcal{J}_7 \mathcal{J}_9$ should be 4, not 2.

E Connection to the distribution function formalism

An alternative formalism for describing redshift-space distortions has been developed in Refs. [16, 70, 71, 90–92], and is known as the distribution function (DF) formalism. In this formalism the redshift space power spectrum is expanded in terms of the velocity moments defined as

$$T_\parallel^L(\mathbf{x}) = (1 + \delta(\mathbf{x}))v_\parallel^L(\mathbf{x}) \quad \text{for} \ \ L \geq 1, \quad \text{and} \ \ T_\parallel^0(\mathbf{x}) = \delta(\mathbf{x}). \tag{E.1}$$

The redshift space power spectrum is then given as

$$P^s(\mathbf{k}) = \sum_{L,L'} \frac{(-1)^{L'}}{L!L'!} \left(\frac{ik_\parallel}{\mathcal{H}}\right)^{L+L'} P_{LL'}(\mathbf{k}), \tag{E.2}$$

where $P_{LL'} = \left\langle T_\parallel^L(\mathbf{k}) \left| T_\parallel^{*L'} \right\rangle\right.'$ are the velocity moment correlators[10].

There is a tight connection between the DF formalism and the GSM. The mean pairwise velocity, v_{12}, corresponds to the density-momentum contribution, P_{01}, to $P(k)$ while the pairwise velocity dispersion, σ_{ij}^2, corresponds to the P_{11} and P_{02} contributions in the distribution function approach. Moreover, expanding the exponent in the GSM and keeping only the terms up to a given PT order one generates all the disconnected contributions to the $P_{LL'}$ correlators (up to the same PT order). In this way, on a basic level, two approaches are equivalent and the difference comes in through the resummation of the connected contributions.

We can show this connection more explicitly. The density momentum correlator, P_{01}, in the DF formalism can be directly related to the pairwise velocity (see also [92]). We have

$$2P_{01,i}(k) = 2\left\langle \delta(k) | \left[1 + \delta(k')\right] \circ u_i(k')\right\rangle' = \int d^3r \ e^{i\mathbf{k}\cdot\mathbf{r}} \left\langle \left[1 + \delta(r)\right]\left[1 + \delta(r')\right]\Delta u_i(r)\right\rangle'$$

$$= \int d^3r \ e^{i\mathbf{k}\cdot\mathbf{r}} \left[1 + \xi(r)\right] v_{12,i}(r). \tag{E.3}$$

or inversely

$$\left[1 + \xi(r)\right] v_{12,i}(r) = 2 \int \frac{d^3k}{(2\pi)^3} e^{-i\mathbf{k}\cdot\mathbf{r}} \ P_{01,i}(k). \tag{E.4}$$

A similar expression holds for the pairwise velocity dispersion, σ_{12}, which we can decompose as

$$\begin{aligned}
\left[1 + \xi(r)\right] \sigma_{12,ij}(r) &= \left\langle \left[1 + \delta\right]\left[1 + \delta'\right]\Delta u_i \Delta u_j' \right\rangle \\
&= 2\left\langle \left[1 + \delta\right]\left[1 + \delta'\right]u_i'u_j'\right\rangle - 2\left\langle \left[1 + \delta\right]u_i\left[1 + \delta'\right]u_j'\right\rangle \\
&= 2\left(\xi_{02}^{ij}(0) + \xi_{02}^{ij}(r) - \xi_{11}^{ij}(r)\right),
\end{aligned} \tag{E.5}$$

where we have introduced correlators

$$\begin{aligned}
\xi_{02}^{ij}(0) &= \left\langle \left[1 + \delta(x)\right]u_i(x)u_j(x)\right\rangle, \\
\xi_{02}^{ij}(r) &= \left\langle \delta(x)\left[1 + \delta(x')\right]u_i(x')u_j(x')\right\rangle, \\
\xi_{11}^{ij}(r) &= \left\langle \left[1 + \delta(x)\right]u_i(x)\left[1 + \delta(x')\right]u_j(x')\right\rangle.
\end{aligned} \tag{E.6}$$

---

[10]For $\langle \ldots \rangle'$ correlators we drop the delta function, and it is to be understood that only the 'on shell' momentum is considered

When Fourier transformed and projected to the line of sight direction $\hat{z}$, these give the momentum-momentum P_{11} and density-energy density P_{02} correlators used in the DF formalism.

If we restrict our comparison to one-loop in PT, all the higher momentum correlators $P_{LL'}$ (P_{12}, P_{03}, P_{13}, P_{04} and P_{22} at one loop) can be reduced to the contributions of irreducible components (cumulants) of terms P_{00}, P_{01}, P_{11} and P_{02} (or equivalently ξ, v_{12} and σ_{12}) [70, 71]. In streaming models these higher momentum correlators (at one loop) correspond to products of cumulants obtained from expansion of the exponent in Eq. (A.6). At higher PT orders these momentum correlators start to collect the nontrivial (irreducible) contributions from the cumulants C, C^i and C^{ij} of Appendix A.

References

[1] D. H. Weinberg, M. J. Mortonson, D. J. Eisenstein, C. Hirata, A. G. Riess, and E. Rozo, *Observational probes of cosmic acceleration*, *PhysRep* **530** (Sept., 2013) 87–255, [arXiv:1201.2434].

[2] **Particle Data Group** Collaboration, K. Olive et al., *Review of Particle Physics*, *Chin.Phys.* **C38** (2014) 090001.

[3] N. Kaiser, *Clustering in real space and in redshift space*, *MNRAS* **227** (July, 1987) 1–21.

[4] A. J. S. Hamilton, *Linear Redshift Distortions: a Review*, in *The Evolving Universe* (D. Hamilton, ed.), vol. 231 of *Astrophysics and Space Science Library*, p. 185, 1998. astro-ph/9708102.

[5] K. S. Dawson, D. J. Schlegel, C. P. Ahn, S. F. Anderson, É. Aubourg, S. Bailey, R. H. Barkhouser, J. E. Bautista, A. Beifiori, A. A. Berlind, V. Bhardwaj, D. Bizyaev, C. H. Blake, M. R. Blanton, M. Blomqvist, A. S. Bolton, A. Borde, J. Bovy, W. N. Brandt, H. Brewington, J. Brinkmann, P. J. Brown, J. R. Brownstein, K. Bundy, N. G. Busca, W. Carithers, A. R. Carnero, M. A. Carr, Y. Chen, J. Comparat, N. Connolly, F. Cope, R. A. C. Croft, A. J. Cuesta, L. N. da Costa, J. R. A. Davenport, T. Delubac, R. de Putter, S. Dhital, A. Ealet, G. L. Ebelke, D. J. Eisenstein, S. Escoffier, X. Fan, N. Filiz Ak, H. Finley, A. Font-Ribera, R. Génova-Santos, J. E. Gunn, H. Guo, D. Haggard, P. B. Hall, J.-C. Hamilton, B. Harris, D. W. Harris, S. Ho, D. W. Hogg, D. Holder, K. Honscheid, J. Huehnerhoff, B. Jordan, W. P. Jordan, G. Kauffmann, E. A. Kazin, D. Kirkby, M. A. Klaene, J.-P. Kneib, J.-M. Le Goff, K.-G. Lee, D. C. Long, C. P. Loomis, B. Lundgren, R. H. Lupton, M. A. G. Maia, M. Makler, E. Malanushenko, V. Malanushenko, R. Mandelbaum, M. Manera, C. Maraston, D. Margala, K. L. Masters, C. K. McBride, P. McDonald, I. D. McGreer, R. G. McMahon, O. Mena, J. Miralda-Escudé, A. D. Montero-Dorta, F. Montesano, D. Muna, A. D. Myers, T. Naugle, R. C. Nichol, P. Noterdaeme, S. E. Nuza, M. D. Olmstead, A. Oravetz, D. J. Oravetz, R. Owen, N. Padmanabhan, N. Palanque-Delabrouille, K. Pan, J. K. Parejko, I. Pâris, W. J. Percival, I. Pérez-Fournon, I. Pérez-Ràfols, P. Petitjean, R. Pfaffenberger, J. Pforr, M. M. Pieri, F. Prada, A. M. Price-Whelan, M. J. Raddick, R. Rebolo, J. Rich, G. T. Richards, C. M. Rockosi, N. A. Roe, A. J. Ross, N. P. Ross, G. Rossi, J. A. Rubiño-Martin, L. Samushia, A. G. Sánchez, C. Sayres, S. J. Schmidt, D. P. Schneider, C. G. Scóccola, H.-J. Seo, A. Shelden, E. Sheldon, Y. Shen, Y. Shu, A. Slosar, S. A. Smee, S. A. Snedden, F. Stauffer, O. Steele, M. A. Strauss, A. Streblyanska, N. Suzuki, M. E. C. Swanson, T. Tal, M. Tanaka, D. Thomas, J. L. Tinker, R. Tojeiro, C. A. Tremonti, M. Vargas Magaña, L. Verde, M. Viel, D. A. Wake, M. Watson, B. A. Weaver, D. H. Weinberg, B. J. Weiner, A. A. West, M. White, W. M. Wood-Vasey, C. Yeche, I. Zehavi, G.-B. Zhao, and Z. Zheng, *The Baryon Oscillation Spectroscopic Survey of SDSS-III*, *AJ* **145** (Jan., 2013) 10, [arXiv:1208.0022].

[6] D. Baumann, A. Nicolis, L. Senatore, and M. Zaldarriaga, *Cosmological non-linearities as an effective fluid*, *JCAP* **7** (July, 2012) 51, [arXiv:1004.2488].

[7] J. J. M. Carrasco, M. P. Hertzberg, and L. Senatore, *The effective field theory of cosmological large scale structures*, *Journal of High Energy Physics* **9** (Sept., 2012) 82, [arXiv:1206.2926].

[8] E. Pajer and M. Zaldarriaga, *On the renormalization of the effective field theory of large scale structures*, *JCAP* **8** (Aug., 2013) 37, [arXiv:1301.7182].

[9] A. Manzotti, M. Peloso, M. Pietroni, M. Viel, and F. Villaescusa-Navarro, *A coarse grained perturbation theory for the Large Scale Structure, with cosmology and time independence in the UV*, *JCAP* **9** (Sept., 2014) 47, [arXiv:1407.1342].

[10] L. Mercolli and E. Pajer, *On the velocity in the Effective Field Theory of Large Scale Structures*, *JCAP* **3** (Mar., 2014) 6, [arXiv:1307.3220].

[11] S. M. Carroll, S. Leichenauer, and J. Pollack, *Consistent effective theory of long-wavelength cosmological perturbations*, *PRD* **90** (July, 2014) 023518, [arXiv:1310.2920].

[12] R. A. Porto, L. Senatore, and M. Zaldarriaga, *The Lagrangian-space Effective Field Theory of large scale structures*, *JCAP* **5** (May, 2014) 022, [arXiv:1311.2168].

[13] Z. Vlah, M. White, and A. Aviles, *A Lagrangian effective field theory*, *JCAP* **9** (Sept., 2015) 014, [arXiv:1506.05264].

[14] J. M. Bardeen, J. R. Bond, N. Kaiser, and A. S. Szalay, *The statistics of peaks of Gaussian random fields*, *ApJ* **304** (May, 1986) 15–61.

[15] B. A. Reid, H.-J. Seo, A. Leauthaud, J. L. Tinker, and M. White, *A 2.5 per cent measurement of the growth rate from small-scale redshift space clustering of SDSS-III CMASS galaxies*, *MNRAS* **444** (Oct., 2014) 476–502, [arXiv:1404.3742].

[16] U. Seljak and P. McDonald, *Distribution function approach to redshift space distortions*, *JCAP* **11** (Nov., 2011) 039, [arXiv:1109.1888].

[17] Y. B. Zel'dovich, *Gravitational instability: An approximate theory for large density perturbations.*, *A&A* **5** (Mar., 1970) 84–89.

[18] T. Buchert, *A class of solutions in Newtonian cosmology and the pancake theory*, *A&A* **223** (Oct., 1989) 9–24.

[19] F. Moutarde, J.-M. Alimi, F. R. Bouchet, R. Pellat, and A. Ramani, *Precollapse scale invariance in gravitational instability*, *ApJ* **382** (Dec., 1991) 377–381.

[20] E. Hivon, F. R. Bouchet, S. Colombi, and R. Juszkiewicz, *Redshift distortions of clustering: a Lagrangian approach.*, *A&A* **298** (June, 1995) 643, [astro-ph/9407049].

[21] A. N. Taylor and A. J. S. Hamilton, *Non-linear cosmological power spectra in real and redshift space*, *MNRAS* **282** (Oct., 1996) 767–778, [astro-ph/9604020].

[22] T. Matsubara, *Resumming cosmological perturbations via the Lagrangian picture: One-loop results in real space and in redshift space*, *PRD* **77** (Mar., 2008) 063530, [arXiv:0711.2521].

[23] T. Matsubara, *Nonlinear perturbation theory with halo bias and redshift-space distortions via the Lagrangian picture*, *PRD* **78** (Oct., 2008) 083519, [arXiv:0807.1733].

[24] J. Carlson, B. Reid, and M. White, *Convolution Lagrangian perturbation theory for biased tracers*, *MNRAS* **429** (Feb., 2013) 1674–1685, [arXiv:1209.0780].

[25] T. Matsubara, *Recursive Solutions of Lagrangian Perturbation Theory*, *ArXiv e-prints* (May, 2015) [arXiv:1505.01481].

[26] V. Zheligovsky and U. Frisch, *Time-analyticity of Lagrangian particle trajectories in ideal fluid flow*, *Journal of Fluid Mechanics* **749** (June, 2014) 404–430, [arXiv:1312.6320].

[27] J. A. Peacock, *Errors on the measurement of Omega via cosmological dipoles*, *MNRAS* **258** (Oct., 1992) 581–586.

[28] C. Park, M. S. Vogeley, M. J. Geller, and J. P. Huchra, *Power spectrum, correlation function, and tests for luminosity bias in the CfA redshift survey*, *ApJ* **431** (Aug., 1994) 569–585.

[29] J. A. Peacock and S. J. Dodds, *Reconstructing the Linear Power Spectrum of Cosmological Mass Fluctuations*, *MNRAS* **267** (Apr., 1994) 1020, [`astro-ph/9311057`].

[30] W. E. Ballinger, J. A. Peacock, and A. F. Heavens, *Measuring the cosmological constant with redshift surveys*, *MNRAS* **282** (Oct., 1996) 877, [`astro-ph/9605017`].

[31] S. Hatton and S. Cole, *Estimating β from redshift-space distortions in the 2dF galaxy survey*, *MNRAS* **310** (Dec., 1999) 1137–1146, [`astro-ph/9905186`].

[32] P. J. E. Peebles, *The large-scale structure of the universe*. 1980.

[33] K. B. Fisher, *On the Validity of the Streaming Model for the Redshift-Space Correlation Function in the Linear Regime*, *ApJ* **448** (Aug., 1995) 494, [`astro-ph/9412081`].

[34] B. A. Reid and M. White, *Towards an accurate model of the redshift-space clustering of haloes in the quasi-linear regime*, *MNRAS* **417** (Nov., 2011) 1913–1927, [`arXiv:1105.4165`].

[35] B. A. Reid, L. Samushia, M. White, W. J. Percival, M. Manera, N. Padmanabhan, A. J. Ross, A. G. Sánchez, S. Bailey, D. Bizyaev, A. S. Bolton, H. Brewington, J. Brinkmann, J. R. Brownstein, A. J. Cuesta, D. J. Eisenstein, J. E. Gunn, K. Honscheid, E. Malanushenko, V. Malanushenko, C. Maraston, C. K. McBride, D. Muna, R. C. Nichol, D. Oravetz, K. Pan, R. de Putter, N. A. Roe, N. P. Ross, D. J. Schlegel, D. P. Schneider, H.-J. Seo, A. Shelden, E. S. Sheldon, A. Simmons, R. A. Skibba, S. Snedden, M. E. C. Swanson, D. Thomas, J. Tinker, R. Tojeiro, L. Verde, D. A. Wake, B. A. Weaver, D. H. Weinberg, I. Zehavi, and G.-B. Zhao, *The clustering of galaxies in the SDSS-III Baryon Oscillation Spectroscopic Survey: measurements of the growth of structure and expansion rate at z = 0.57 from anisotropic clustering*, *MNRAS* **426** (Nov., 2012) 2719–2737, [`arXiv:1203.6641`].

[36] L. Wang, B. Reid, and M. White, *An analytic model for redshift-space distortions*, *MNRAS* **437** (Jan., 2014) 588–599, [`arXiv:1306.1804`].

[37] D. Bianchi, M. Chiesa, and L. Guzzo, *Improving the modelling of redshift-space distortions - I. A bivariate Gaussian description for the galaxy pairwise velocity distributions*, *MNRAS* **446** (Jan., 2015) 75–84, [`arXiv:1407.4753`].

[38] D. Bianchi, W. Percival, and J. Bel, *Improving the modelling of redshift-space distortions - II. A pairwise velocity model covering large and small scales*, *ArXiv e-prints* (Feb., 2016) [`arXiv:1602.02780`].

[39] C. Uhlemann, M. Kopp, and T. Haugg, *Edgeworth streaming model for redshift space distortions*, *PRD* **92** (Sept., 2015) 063004, [`arXiv:1503.08837`].

[40] M. Kopp, C. Uhlemann, and I. Achitouv, *Choose to smooth: Gaussian streaming with the truncated Zel'dovich approximation*, *ArXiv e-prints* (June, 2016) [`arXiv:1606.02301`].

[41] Z. Vlah, U. Seljak, and T. Baldauf, *Lagrangian perturbation theory at one loop order: Successes, failu res, and improvements*, *PRD* **91** (Jan., 2015) 023508, [`arXiv:1410.1617`].

[42] F. Bernardeau, S. Colombi, E. Gaztañaga, and R. Scoccimarro, *Large-scale structure of the Universe and cosmological perturbation theory*, *PhysRep* **367** (Sept., 2002) 1–248, [`astro-ph/0112551`].

[43] R. Takahashi, *Third-Order Density Perturbation and One-Loop Power Spectrum in Dark-Energy-Dominated Universe*, *Progress of Theoretical Physics* **120** (Sept., 2008) 549–559, [`arXiv:0806.1437`].

[44] M. Fasiello and Z. Vlah, *Non-linear Fields in Generalized Cosmologies*, *ArXiv e-prints* (Apr., 2016) [`arXiv:1604.04612`].

[45] P. Catelan, F. Lucchin, S. Matarrese, and C. Porciani, *The bias field of dark matter haloes*, *MNRAS* **297** (July, 1998) 692–712, [astro-ph/9708067].

[46] P. Catelan, C. Porciani, and M. Kamionkowski, *Two ways of biasing galaxy formation*, *MNRAS* **318** (Nov., 2000) L39–L44, [astro-ph/0005544].

[47] P. McDonald and A. Roy, *Clustering of dark matter tracers: generalizing bias for the coming era of precision LSS*, *JCAP* **8** (Aug., 2009) 020, [arXiv:0902.0991].

[48] V. Desjacques, M. Crocce, R. Scoccimarro, and R. K. Sheth, *Modeling scale-dependent bias on the baryonic acoustic scale with the statistics of peaks of Gaussian random fields*, *PRD* **82** (Nov., 2010) 103529, [arXiv:1009.3449].

[49] M. Musso, A. Paranjape, and R. K. Sheth, *Scale-dependent halo bias in the excursion set approach*, *MNRAS* **427** (Dec., 2012) 3145–3158, [arXiv:1205.3401].

[50] K. C. Chan, R. Scoccimarro, and R. K. Sheth, *Gravity and large-scale nonlocal bias*, *PRD* **85** (Apr., 2012) 083509, [arXiv:1201.3614].

[51] T. Baldauf, U. Seljak, V. Desjacques, and P. McDonald, *Evidence for quadratic tidal tensor bias from the halo bispectrum*, *PRD* **86** (Oct., 2012) 083540, [arXiv:1201.4827].

[52] F. Schmidt, D. Jeong, and V. Desjacques, *Peak-background split, renormalization, and galaxy clustering*, *PRD* **88** (July, 2013) 023515, [arXiv:1212.0868].

[53] A. Paranjape, E. Sefusatti, K. C. Chan, V. Desjacques, P. Monaco, and R. K. Sheth, *Bias deconstructed: unravelling the scale dependence of halo bias using real-space measurements*, *MNRAS* **436** (Nov., 2013) 449–459, [arXiv:1305.5830].

[54] M. White, *The Zel'dovich approximation*, *MNRAS* **439** (Apr., 2014) 3630–3640, [arXiv:1401.5466].

[55] T. Matsubara and V. Desjacques, *Impacts of biasing schemes in the one-loop integrated perturbation theory*, *PRD* **93** (June, 2016) 123522, [arXiv:1604.06579].

[56] V. Assassi, D. Baumann, D. Green, and M. Zaldarriaga, *Renormalized halo bias*, *JCAP* **8** (Aug., 2014) 056, [arXiv:1402.5916].

[57] L. Senatore, *Bias in the effective field theory of large scale structures*, *JCAP* **11** (Nov., 2015) 007, [arXiv:1406.7843].

[58] M. Mirbabayi, F. Schmidt, and M. Zaldarriaga, *Biased tracers and time evolution*, *JCAP* **7** (July, 2015) 030, [arXiv:1412.5169].

[59] R. Angulo, M. Fasiello, L. Senatore, and Z. Vlah, *On the statistics of biased tracers in the Effective Field Theory of Large Scale Structures*, *JCAP* **9** (Sept., 2015) 029, [arXiv:1503.08826].

[60] T. Fujita, V. Mauerhofer, L. Senatore, Z. Vlah, and R. Angulo, *Very Massive Tracers and Higher Derivative Biases*, *ArXiv e-prints* (Sept., 2016) [arXiv:1609.00717].

[61] S. Saito, T. Baldauf, Z. Vlah, U. Seljak, T. Okumura, and P. McDonald, *Understanding higher-order nonlocal halo bias at large scales by combining the power spectrum with the bispectrum*, *PRD* **90** (Dec., 2014) 123522, [arXiv:1405.1447].

[62] M. Biagetti, V. Desjacques, A. Kehagias, and A. Riotto, *Nonlocal halo bias with and without massive neutrinos*, *Phys. Rev.* **D90** (2014), no. 4 045022, [arXiv:1405.1435].

[63] V. Desjacques, *Baryon acoustic signature in the clustering of density maxima*, *PRD* **78** (Nov., 2008) 103503, [arXiv:0806.0007].

[64] A. Paranjape, R. K. Sheth, and V. Desjacques, *Excursion set peaks: a self-consistent model of dark halo abundances and clustering*, *MNRAS* **431** (May, 2013) 1503–1512, [arXiv:1210.1483].

[65] R. K. Sheth, K. C. Chan, and R. Scoccimarro, *Nonlocal Lagrangian bias*, *PRD* **87** (Apr., 2013) 083002, [arXiv:1207.7117].

[66] T. Baldauf, V. Desjacques, and U. Seljak, *Velocity bias in the distribution of dark matter halos*, *PRD* **92** (Dec., 2015) 123507, [arXiv:1405.5885].

[67] M. Schmittfull, Z. Vlah, and P. McDonald, *Fast Large Scale Structure Perturbation Theory using 1D FFTs*, *ArXiv e-prints* (Mar., 2016) [arXiv:1603.04405].

[68] M. Schmittfull and Z. Vlah, *FFT-PT: Reducing the 2-loop large-scale structure power spectrum to one-dimensional, radial integrals*, *ArXiv e-prints* (Sept., 2016) [arXiv:1609.00349].

[69] L. Senatore and M. Zaldarriaga, *The IR-resummed Effective Field Theory of Large Scale Structures*, *JCAP* **2** (Feb., 2015) 13, [arXiv:1404.5954].

[70] Z. Vlah, U. Seljak, P. McDonald, T. Okumura, and T. Baldauf, *Distribution function approach to redshift space distortions. Part IV: perturbation theory applied to dark matter*, *JCAP* **11** (Nov., 2012) 009, [arXiv:1207.0839].

[71] Z. Vlah, U. Seljak, T. Okumura, and V. Desjacques, *Distribution function approach to redshift space distortions. Part V: perturbation theory applied to dark matter halos*, *JCAP* **10** (Oct., 2013) 053, [arXiv:1308.6294].

[72] U. Seljak and Z. Vlah, *Halo Zel'dovich model and perturbation theory: Dark matter power spectrum and correlation function*, *PRD* **91** (June, 2015) 123516, [arXiv:1501.07512].

[73] J. R. Bond and H. M. P. Couchman, $w_{gg}(\theta)$ *as a probe of large scale structure.*, in *Proceedings of the 2nd Canadian Conference on General Relativity and Relativistic Astrophysics* (A. Coley, C. Dyer, and T. Tupper, eds.), pp. 385–389, 1988.

[74] K. B. Fisher and A. Nusser, *The non-linear redshift-space power spectrum: Omega from redshift surveys*, *MNRAS* **279** (Mar., 1996) L1–L5, [astro-ph/9510049].

[75] S. Tassev, *N-point statistics of large-scale structure in the Zel'dovich approximation*, *JCAP* **6** (June, 2014) 012, [arXiv:1311.6316].

[76] N. Kaiser, *On the spatial correlations of Abell clusters*, *ApJL* **284** (Sept., 1984) L9–L12.

[77] S. Cole and N. Kaiser, *Biased clustering in the cold dark matter cosmogony*, *MNRAS* **237** (Apr., 1989) 1127–1146.

[78] H. J. Mo and S. D. M. White, *An analytic model for the spatial clustering of dark matter haloes*, *MNRAS* **282** (Sept., 1996) 347–361, [astro-ph/9512127].

[79] R. K. Sheth and G. Tormen, *Large-scale bias and the peak background split*, *MNRAS* **308** (Sept., 1999) 119–126, [astro-ph/9901122].

[80] S. Matarrese, P. Coles, F. Lucchin, and L. Moscardini, *Redshift evolution of clustering*, *MNRAS* **286** (Mar., 1997) 115–132, [astro-ph/9608004].

[81] M. White, P. Martini, and J. D. Cohn, *Constraints on the correlation between QSO luminosity and host halo mass from high-redshift quasar clustering*, *MNRAS* **390** (Nov., 2008) 1179–1184, [arXiv:0711.4109].

[82] M. White, B. Reid, C.-H. Chuang, J. L. Tinker, C. K. McBride, F. Prada, and L. Samushia, *Tests of redshift-space distortions models in configuration space for the analysis of the BOSS final data release*, *MNRAS* **447** (Feb., 2015) 234–245, [arXiv:1408.5435].

[83] T. Baldauf, L. Mercolli, and M. Zaldarriaga, *Effective field theory of large scale structure at two loops: The apparent scale dependence of the speed of sound*, *PRD* **92** (Dec., 2015) 123007, [arXiv:1507.02256].

[84] T. Sunayama, N. Padmanabhan, K. Heitmann, S. Habib, and E. Rangel, *Efficient construction of mock catalogs for baryon acoustic oscillation surveys*, *JCAP* **5** (May, 2016) 051, [arXiv:1510.06665].

[85] M. Davis, G. Efstathiou, C. S. Frenk, and S. D. M. White, *The evolution of large-scale structure in a universe dominated by cold dark matter*, *ApJ* **292** (May, 1985) 371–394.

[86] A. Lewis, A. Challinor, and A. Lasenby, *Efficient computation of CMB anisotropies in closed FRW models*, *Astrophys. J.* **538** (2000) 473–476, [`astro-ph/9911177`].

[87] T. Okumura, N. Hand, U. Seljak, Z. Vlah, and V. Desjacques, *Galaxy power spectrum in redshift space: Combining perturbation theory with the halo model*, *PRD* **92** (Nov., 2015) 103516, [`arXiv:1506.05814`].

[88] M. White, *Reconstruction within the Zeldovich approximation*, *MNRAS* **450** (July, 2015) 3822–3828, [`arXiv:1504.03677`].

[89] A. J. S. Hamilton, *Uncorrelated modes of the non-linear power spectrum*, *MNRAS* **312** (Feb., 2000) 257–284, [`astro-ph/9905191`].

[90] T. Okumura, U. Seljak, P. McDonald, and V. Desjacques, *Distribution function approach to redshift space distortions. Part II: N-body simulations*, *JCAP* **2** (Feb., 2012) 010, [`arXiv:1109.1609`].

[91] T. Okumura, U. Seljak, and V. Desjacques, *Distribution function approach to redshift space distortions. Part III: halos and galaxies*, *JCAP* **11** (Nov., 2012) 014, [`arXiv:1206.4070`].

[92] T. Okumura, U. Seljak, Z. Vlah, and V. Desjacques, *Peculiar velocities in redshift space: formalism, N-body simulations and perturbation theory*, *JCAP* **5** (May, 2014) 003, [`arXiv:1312.4214`].